

Technische Universität  
München  
Physik-Department



**The Decays  $B \rightarrow X_s \gamma$ ,  
 $B \rightarrow X_s$  gluon and  $B \rightarrow X_s \mu^+ \mu^-$   
in Universal Extra Dimensions  
and Mass Corrections in  
Dimensional Deconstruction**

Dissertation

von

**Michael Spranger**

Max-Planck-Institut für Physik  
(Werner-Heisenberg-Institut)  
Föhringer Ring 6  
D-80805 München  
Email: [spranger@mppmu.mpg.de](mailto:spranger@mppmu.mpg.de)

Max-Planck-Institut  
für Physik  
(Werner-Heisenberg-Institut)





**Physik-Department**  
**Technische Universität München**  
Institut für Theoretische Physik  
Lehrstuhl Univ.-Prof. Dr. Andrzej J. Buras

**The Decays  $B \rightarrow X_s \gamma$ ,  
 $B \rightarrow X_s$  gluon and  $B \rightarrow X_s \mu^+ \mu^-$   
in Universal Extra Dimensions  
and Mass Corrections in  
Dimensional Deconstruction**

Michael Spranger

Vollständiger Abdruck der von der Fakultät für Physik der Technischen Universität München zur Erlangung des akademischen Grades eines

**Doktors der Naturwissenschaften (Dr. rer. nat.)**

genehmigten Dissertation.

Vorsitzender: Univ.-Prof. Dr. F. von Feilitzsch

Prüfer der Dissertation: 1. Univ.-Prof. Dr. A. J. Buras

2. Univ.-Prof. Dr. M. Lindner

Die Dissertation wurde am 11.10.2005 bei der Technischen Universität München eingereicht und durch die Fakultät für Physik am 25.10.2005 angenommen.



**Meiner Mutter**



# Abstract

In this thesis an extension of the Standard Model of particle physics in Universal Extra Dimensions (UED) is discussed. The flavour-changing neutral current (FCNC) decays  $B \rightarrow X_s \gamma$ ,  $B \rightarrow X_s$  gluon and  $B \rightarrow X_s \mu^+ \mu^-$  are used to constrain the compactification scale  $1/R$  in the model introduced by Appelquist, Cheng and Dobrescu (ACD). Values of  $1/R \geq 300$  GeV are found to be consistent with experimental data.

In addition, the ultraviolet completion of UED models in the framework of Dimensional Deconstruction is investigated. In particular, the realization of chiral fermions and the issue of Kaluza-Klein parity is discussed. The calculated radiative corrections of fermion masses permit to draw conclusions on the renormalizability and structure of the fundamental Lagrangian. Moreover, the running contribution to the fermion masses from the cut-off scale is extracted and compared to the result in the corresponding continuum theory.





# Contents

<b>1</b>	<b>Introduction</b>	<b>9</b>
<b>2</b>	<b>Technicalities</b>	<b>15</b>
2.1	Effective Field Theories . . . . .	16
2.2	Dimensional Regularization . . . . .	17
2.3	Renormalization . . . . .	19
2.4	The Renormalization Group . . . . .	22
<b>3</b>	<b>Flavour physics</b>	<b>25</b>
3.1	Penguin Diagrams in the ACD Model . . . . .	26
3.1.1	Effective vertices . . . . .	26
3.1.2	General Structure of the Calculation . . . . .	27
3.1.3	The functions $D, E, D', E'$ and $Z$ . . . . .	29
3.2	The decays $B \rightarrow X_s \gamma$ and $B \rightarrow X_s$ gluon . . . . .	34
3.2.1	Effective Hamiltonian . . . . .	34
3.2.2	Branching Ratio for $B \rightarrow X_s \gamma$ . . . . .	35
3.2.3	Branching Ratio for $B \rightarrow X_s$ gluon . . . . .	37
3.3	The decay $B \rightarrow X_s \mu^+ \mu^-$ . . . . .	39
3.3.1	Effective Hamiltonian and Branching Ratio . . . . .	39
3.3.2	Forward-Backward Asymmetry . . . . .	41
<b>4</b>	<b>Dimensional Deconstruction</b>	<b>45</b>
4.1	Framework . . . . .	46
4.1.1	Gauge field lattice . . . . .	46
4.1.2	Fermions in the aliphatic setup . . . . .	49
4.2	Feynman rules and Kaluza-Klein parity . . . . .	53
4.3	Fermion counter terms and mass shift . . . . .	58
<b>5</b>	<b>Conclusions</b>	<b>63</b>
5.1	Conclusions . . . . .	64
<b>A</b>	<b>Background Field Method in 5 Dimensions</b>	<b>69</b>

<b>B</b>	<b>Feynman Rules in the ACD Model: Photon and Gluons</b>	<b>73</b>
<b>C</b>	<b>Useful formulae</b>	<b>77</b>
C.1	Orthogonality relations . . . . .	77
C.2	Vertex sums . . . . .	77
C.3	Sum in the $\bar{\psi}_L A \psi_L$ vertex . . . . .	78
<b>D</b>	<b>Fermion self-energy</b>	<b>79</b>
	<b>Bibliography</b>	<b>83</b>
	<b>Acknowledgments</b>	<b>89</b>

# Chapter 1

## Introduction

The Standard Model (SM) of elementary particle physics has been established as the basis of the phenomenological description of high-energy physics. It accounts for all elementary particles discovered so far and their interactions according to the gauge principle as well as Yukawa interactions between fermions and the Higgs field. The flavour structure in the quark sector is described by the Cabibbo-Kobayashi-Maskawa (CKM) matrix, and electroweak symmetry breaking is conveniently described by the Higgs mechanism.

Up to the present day, all experimental data in particle physics, with the exception of neutrino oscillations, are fully explained and consistent within errors with the description of nature by the SM. In spite of this tremendous success, it is commonly believed for several reasons that the SM is not the final answer. The SM is a renormalizable quantum field theory, and its parameters have to be determined by experiment. However, we do not understand the origin of the mass hierarchies in the quark and lepton sector and the corresponding mixing patterns. In particular, it is unclear why there exist quarks and leptons much lighter than the electroweak scale. We do not understand the mechanism of electroweak symmetry breaking that is responsible for the generation of these masses and the hierarchy between the electroweak scale and the Planck scale. In addition, the values of the different gauge couplings may appear arbitrary and not correlated at low energies. Furthermore, the attempts to reconcile gravity with quantum mechanics have been elusive up to the present. It is therefore expected that our current description of nature breaks down at the Planck scale where gravitational effects are no longer negligible in the interactions of elementary particles.

From these arguments, it is clear that the SM cannot be the ultimate description of nature. In fact it can be argued quite generally that any physical theory comprising quantum mechanics and special relativity will look like a relativistic quantum field theory at low energies. Despite its renormalizability, the SM is merely an effective theory valid at energies accessible at present-day colliders, with deviations accounted for by the inclusion of higher dimensional operators.

A promising framework for new physics is the extension of the SM to more than the common four dimensions of space-time. In recent years there has been an increasing interest in those models, motivated by the demand of extra dimensions in string theory and specifically the possibility of a compactification scale in the TeV range [1]. At low energies, the relevant degrees of freedom are towers of Kaluza-Klein (KK) excitations of the Standard Model particles.

Orbifold compactifications are used to realize chiral fermions and build models that look like the Standard Model at low energies. The simplest possibility is one extra dimension with the geometry of  $S^1/Z_2$  where translational Lorentz symmetry is broken at the two fixed points.

A special role among extra dimensional models is played by those with universal extra dimensions (UED), where all SM fields live in all available dimensions. The model introduced by Appelquist, Cheng and Dobrescu (ACD) [2] consists of one universal extra dimension compactified to the orbifold  $S^1/Z_2$ . Compared to the SM, the only additional free parameter is the compactification radius  $1/R$ . All masses of the KK particles and

their interactions are described in terms of  $1/R$  and the SM parameters.

A very important property of the ACD model is the conservation of KK parity which implies the absence of tree-level contributions beyond those already present in the SM. Processes which are forbidden at the classical level are a particularly useful probe for extensions of the SM. Such processes are induced by quantum effects and the effect of new physics could be similar in size. Since flavour-changing neutral current (FCNC) processes are induced radiatively, they are particularly interesting in this respect. In [3] the contributions of the KK modes to the  $K_L - K_S$  mass difference  $\Delta M_K$ , the parameter  $\varepsilon_K$ , the  $B_{d,s}^0 - \bar{B}_{d,s}^0$  mixing mass differences  $\Delta M_{d,s}$  and the rare decays  $K^+ \rightarrow \pi^+ \nu \bar{\nu}$ ,  $K_L \rightarrow \pi^0 \nu \bar{\nu}$ ,  $K_L \rightarrow \mu^+ \mu^-$ ,  $B \rightarrow X_{s,d} \nu \bar{\nu}$  and  $B_{s,d} \rightarrow \mu^+ \mu^-$  were calculated. It was found that the effects are significant in processes governed by the CKM element  $|V_{ts}|$  like  $B \rightarrow X_s \nu \bar{\nu}$  and  $B_s \rightarrow \mu^+ \mu^-$ , in which the enhancement through the KK modes in  $Z^0$  penguin diagrams is not softened by the suppression of the relevant CKM parameters in contrast to the processes governed by  $|V_{td}|$ .

The calculation of the  $\gamma$  penguins, gluon penguins,  $\gamma$ -magnetic penguins and chromo-magnetic penguins in this thesis allow the study of further processes. Here we analyse in detail the impact of the KK contributions on the decays  $B \rightarrow X_s \gamma$ ,  $B \rightarrow X_s$  gluon and  $B \rightarrow X_s \mu^+ \mu^-$ . Among these processes only the decay  $B \rightarrow X_s \gamma$  has been so far considered in the ACD model in the literature [4]. As we will see our results are consistent with the ones obtained by these authors. However, we have included the numerically relevant next-to-leading order QCD corrections which are indispensable for a reliable phenomenological analysis, along with an accurate treatment of the theoretical and experimental uncertainties.

With the calculation of the penguin diagrams in this work together with the results in [3], it is also possible to analyse the decay  $K_L \rightarrow \pi^0 e^+ e^-$  and the CP-violating ratio  $\varepsilon'/\varepsilon$ . Unfortunately, for the decay  $K_L \rightarrow \pi^0 e^+ e^-$  there exists only an upper bound on the branching ratio [5] which is still by two orders of magnitude away from the SM and ACD model expectations, while for the ratio  $\varepsilon'/\varepsilon$  hadronic uncertainties in the lattice calculation are still substantial. Because of these obstacles both observables are presently not suited for the extraction of the compactification radius  $1/R$  from the data [6].

Also other processes of interest have been investigated in the framework of universal extra dimensions. From precision electroweak observables the lower bounds  $1/R \geq 300$  GeV and  $1/R \geq 250$  GeV have been established for a light Higgs with  $m_H \leq 250$  GeV and a heavy Higgs, respectively [2, 7]. In [8] vacuum stability in a simplified ACD model has been examined. Also the investigation of the anomalous magnetic moment of the muon [9] and of the  $Z \rightarrow b\bar{b}$  vertex [3, 10] are consistent with a compactification scale of  $1/R \geq 300$  GeV.

Quantum field theories with extra dimensions are generally not renormalizable, which is also the case for the ACD model. They have to be taken as effective theories valid below some cut-off scale  $\Lambda$ . The physics above this cut-off is a priori not determined but can in principle be accounted for by non-renormalizable operators, giving contributions to low-energy observables suppressed by powers of  $1/\Lambda$ .

If the cut-off is implemented by a truncation of the KK modes, several difficulties arise. This naive approach violates local gauge invariance in the extra dimensions. Moreover, without a definite renormalizable ultra-violet (UV) completion, the influence of the physics above the cut-off scale remains undetermined.

Extra dimensions emerge dynamically in dimensional deconstruction [11, 12]. Here a given theory can be associated with a moose diagram in theory space consisting of sites and links. Dimensional deconstruction can serve as a renormalizable, gauge invariant UV completion for extra dimensional theories. It acts as a regulator, where the extra dimensions are replaced by a discrete lattice providing a natural cut-off. Dimensional deconstruction also stands on its own right as a framework for building models that do not necessarily correspond in any way to extra dimensions. The applications of dimensional deconstruction comprise topics such as electroweak symmetry breaking, gauge coupling unification and GUT theories, supersymmetry, gravity and warped geometries [14, 15, 16, 17, 18, 19, 20].

In dimensional deconstruction, the orbifold  $S^1/Z_2$  is modelled by an aliphatic setup with chiral fermions. In theory space this geometry is represented by a line, with its two endpoints corresponding to the fixed points of the orbifold. In this thesis we investigate which properties of the higher dimensional orbifold models are reproduced in the deconstructed aliphatic setup with fermions in the bulk.

The parameters of the deconstructed theory are matched to those of the continuous theory so as to yield the same mass spectrum and couplings at low energies. In order to be a faithful low energy representation of a higher dimensional field theory, also the Feynman rules have to be equivalent and characteristic properties like KK parity have to be reproduced. We will elaborate on the Feynman rules in the aliphatic setup and point out the differences to the continuum, in particular the violation of KK parity.

In orbifold models quantum loop effects produce infinite contributions that require renormalization by introducing couplings at the fixed points [26]. These brane couplings arise from integrals over the 4-dimensional momentum running inside the loop and thus are given by the cut-off of the 4-dimensional theory. Since the deconstructed models are designed to reproduce the higher dimensional models in the low-energy regime, it is interesting to study how loop corrections affect the renormalization of couplings at the individual lattice sites. We will show that an additional counterterm needs to be introduced at one endpoint of the lattice. In addition, we will demonstrate how loop corrections substantiate the naturalness problem of the fermionic mass spectrum that is already present at the tree level.

One-loop corrections to the masses of the KK excitations in dimensional deconstruction were calculated for Yang-Mills gauge theories [22], in supersymmetric models [23, 24] and for the KK gauge boson excitations in deconstructed 5-dimensional QED compactified on a circle [25]. Assuming vanishing boundary terms at the cut-off scale, the divergent parts of the self-energy diagrams give the running mass correction between the cut-off scale and the renormalization scale. We compute these contributions in the aliphatic model with fermions in the bulk and compare our findings to the result obtained in the ACD

model [21].

This thesis is organized as follows. In Chapter 2 we give an introduction into the technical tools needed for the phenomenological discussion of  $B$  meson decays and the comprehension of the role dimensional deconstruction plays as an effective theory for extra dimensional models. We discuss effective field theories, regularization methods, renormalization and the renormalization group. We take a closer look at the renormalization of the flavour changing vertex  $\bar{s}A^\mu b$  which is important for the internal consistency of the calculation of the radiative weak decays in this thesis.

In Chapter 3 we address the impact of the KK modes on the FCNC decays  $B \rightarrow X_s \gamma$ ,  $B \rightarrow X_s$  gluon and  $B \rightarrow X_s \mu^+ \mu^-$ . We start with the discussion of the penguin diagrams involved in the calculation and show the effective vertices that contribute to the processes. Then we expose the general structure of the calculation and present the resulting Inami-Lim functions in the ACD model. Next we discuss the impact of the KK modes on the branching ratios of the decays  $B \rightarrow X_s \gamma$  and  $B \rightarrow X_s$  gluon. The last section deals with the decay  $B \rightarrow X_s \mu^+ \mu^-$  where we analyse the branching ratio and the forward-backward asymmetry.

The dimensional deconstruction of universal extra dimensions is discussed in Chapter 4. We start by introducing the framework of gauge fields and fermions on the aliphatic lattice. Next we take a closer look at the Feynman rules of the model and the issue of Kaluza-Klein parity. Then we compute the renormalization of fermion masses and the associated counter terms.

In the final chapter we summarize our results and give a short outlook. In the appendices, we discuss some technical details of this work. In Appendix A the application of the method of background fields to universal extra dimensions is discussed. We present the relevant Feynman rules of the ACD model in background field gauge in Appendix B. Relevant formulae for the derivation of the Feynman rules in the aliphatic model are collected in Appendix C. Finally the contributions of the various diagrams contributing to the fermion self-energy are given in Appendix D, which concludes this thesis.





## Chapter 2

# Technicalities

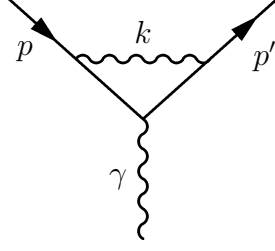


Figure 2.1: One-loop vertex correction to the electron scattering off a photon.

## 2.1 Effective Field Theories

The basic idea of effective field theories is that all effects of possibly unknown high-energy physics can be simulated by a new set of local interactions. The states with energy greater than a certain cut-off are discarded from the theory. Their effect on low-energy physics is accounted for by the coefficients of the old and new interactions in the Lagrangian. The change of coefficients in the Lagrangian through this procedure is called renormalization.

As an example, we show the renormalization of the electric charge in QED defined by the Lagrangian

$$\mathcal{L}_0 = \bar{\psi}(i\cancel{\partial} - e_0\cancel{A} - m_0)\psi - \frac{1}{4}F_{\mu\nu}F^{\mu\nu}. \quad (2.1)$$

Here we assume that the theory is regulated by a cut-off  $\Lambda_0$  up to which all loop integrations are performed. From this theory, we now remove all states having energy or momenta larger than some new cutoff  $\Lambda$ . The scattering for an electron off an external vector field is at one-loop level described by Fig. 2.1. The part of the amplitude that is discarded is given by

$$\begin{aligned} \mathcal{A}(\Lambda < k < \Lambda_0) &= -e_0^3 \int_{\Lambda}^{\Lambda_0} \frac{d^4k}{(2\pi)^4} \frac{g^{\mu\nu}}{k^2} \\ &\times \bar{u}(p')\gamma_{\mu} \frac{(\not{p}' - \not{k}) + m_0}{(p' - k)^2 - m_0^2} \cancel{A}_{\text{ext}} \frac{(\not{p} - \not{k}) + m_0}{(p - k)^2 - m_0^2} \gamma_{\nu} u(p). \end{aligned} \quad (2.2)$$

We can simplify the integral by neglecting  $p, p'$  and  $m_0$  which are assumed to be much less than  $\Lambda$ :

$$\mathcal{A}(\Lambda < k < \Lambda_0) = -e_0^3 \bar{u}(p') \cancel{A}_{\text{ext}} u(p) \int_{\Lambda}^{\Lambda_0} \frac{d^4k}{(2\pi)^4} \frac{1}{(k^2)^2}. \quad (2.3)$$

Also including the other one-loop corrections, we find that the discarded part of the electron scattering amplitude is given by

$$\mathcal{A}(\Lambda < k < \Lambda_0) = -e_0 c_1 (\Lambda/\Lambda_0) \bar{u}(p') \cancel{A}_{\text{ext}} u(p), \quad (2.4)$$

where the dimensionless constant  $c_1(\Lambda/\Lambda_0)$  is given by

$$c_1(\Lambda/\Lambda_0) = -\frac{\alpha_0}{6\pi} \log \frac{\Lambda}{\Lambda_0}. \quad (2.5)$$

Such a contribution can be reincorporated into the theory by adding the new interaction

$$\delta\mathcal{L}_0 = -e_0 c_1(\Lambda/\Lambda_0) \bar{\psi} \not{A} \psi \quad (2.6)$$

to the Lagrangian. This amounts to a redefinition of the electric charge

$$e = e_0 + \delta e_0, \quad (2.7)$$

$$\delta e_0 = e_0 c_1(\Lambda/\Lambda_0), \quad (2.8)$$

where  $e$  is the renormalized value.

Other processes require further interactions in the Lagrangian. For example for the electron-electron scattering, the analogous modification of the Lagrangian is given by

$$\delta\mathcal{L}_0 = c_2(\Lambda/\Lambda_0) \frac{1}{\Lambda^2} \bar{\psi} \gamma_\mu \psi \bar{\psi} \gamma^\mu \psi. \quad (2.9)$$

Generally, the omission of states beyond the cut-off can be represented as an expansion in  $p/\Lambda$ . This follows from the uncertainty principle. From the low-energy point of view ( $p \ll \Lambda$ ), interactions involving intermediate states with energy and momenta greater than the cut-off are local, since they are highly virtual and therefore short-lived. This locality is reflected in the fact that the contributions to all processes can be accounted for by terms that are polynomial in fields and derivatives.

## 2.2 Dimensional Regularization

In practical calculations, it is often convenient not to work with a cut-off  $\Lambda_0$ . Such an explicit cut-off can cause problems, since it is violating gauge invariance and possibly other important symmetries. A regulation procedure preserving gauge invariance symmetries is dimensional regularization. Here the loop integration is performed in  $d = 2 - \epsilon$  dimension, where  $\epsilon$  can be an arbitrary complex number.

Technically, this is achieved in a two-step procedure. As the first step, the loop integrals are evaluated in integer dimension  $d$ , where  $d$  is chosen such that the loop integral converges. A typical one-loop integral is given by

$$\int \frac{d^d l_E}{(2\pi)^d} \frac{1}{(l_E + \Delta)^2} = \frac{1}{(4\pi)^{d/2}} \frac{\Gamma(2 - d/2)}{\Gamma(2)} \left(\frac{1}{\Delta}\right)^{2-d/2}, \quad (2.10)$$

where  $\Gamma(z)$  is the Euler gamma function with isolated poles at  $z = 0, -1, -2, \dots$ , and  $\Delta$  is a function of masses and external momenta.<sup>1</sup> We also have to introduce a renormalization

<sup>1</sup>Note that for  $d = 4$  the integral diverges.

scale  $\mu$  in order to maintain dimensionless coupling constants. In the case of QED, this would be done by

$$e \rightarrow e\mu^{2-d/2}. \quad (2.11)$$

In the second step, the result expressed in terms of  $d$  is analytically continued to arbitrary  $d = 2 - \epsilon$ . The Euler gamma function is expanded around the poles in integer dimensions via the identity

$$\Gamma(\epsilon) = \frac{1}{\epsilon} - \gamma_E + \mathcal{O}(\epsilon), \quad (2.12)$$

where  $\gamma_E = 0.5772\dots$  is the Euler-Mascheroni constant. With this identity, the integral can be expanded around  $d = 4$ :

$$\int \frac{d^d l_E}{(2\pi)^d} \frac{1}{(l_E + \Delta)^2} \rightarrow \frac{1}{(4\pi)^2} \left( \frac{1}{\epsilon} - \log \Delta - \gamma_E + \log 4\pi + \mathcal{O}(\epsilon) \right). \quad (2.13)$$

In a renormalizable theory, for observable quantities all poles  $1/\epsilon$  must cancel after renormalization of the parameters of the Lagrangian, yielding a finite and well-defined result.

For the renormalization of Feynman amplitudes, we must specify some renormalization conditions. In dimensional regularization, two convenient renormalization schemes are the MS and the  $\overline{\text{MS}}$  scheme. In the MS scheme the fields and parameters in the Lagrangian are redefined to solely cancel the  $1/\epsilon$  poles. The  $\overline{\text{MS}}$  scheme differs from the MS scheme by a redefinition of the renormalization scale

$$\mu_{\overline{\text{MS}}} = \mu e^{\gamma_E/2} (4\pi)^{-1/2}, \quad (2.14)$$

with the effect of also eliminating the unphysical terms  $\gamma_E + \log 4\pi$ .

Undoubtedly, there are several advantages that make dimensional regularization in combination with the  $\overline{\text{MS}}$  scheme a very convenient choice in practical calculations:

- It leads to simpler expressions in the loop integrals, which makes the calculations easier than in other regularization schemes.
- The divergencies are subtracted automatically, while physical renormalization conditions are generally more complicated to implement.
- The renormalization group functions are independent of  $\mu$ , since it is a mass-independent subtraction scheme.

However, there also arise several drawbacks which require special care:

- Dimensional regularization not only affects physics at high energies, but can modify it at large distances as well, and is therefore, in general, not a sensible regulator.

- Ultra-Violet (UV) and Infra-Red (IR) divergencies can mix, in which case they usually have to be separated by introducing regulator masses for massless particles.
- The Appelquist-Carazone decoupling theorem [27] does not work in a mass-independent scheme [28]. To deal with this problem, the best solution is to use effective field theory. The physics of the Appelquist-Carazone theorem is put in by hand by explicitly integrating out the heavy particles.
- There is no entirely satisfactory way of defining  $\gamma_5$  in non-integer dimensions [29, 30]. For practical calculations in non-supersymmetric theories, the most convenient choice is the “naive dimensional regularization” (NDR) scheme, although expressions like  $\text{Tr}(\gamma_5\gamma_\mu\gamma_\nu\gamma_\rho\gamma_\lambda)$  are not unambiguously defined. If it is not possible to avoid such expressions, one must resort to other schemes, for example the one proposed by 't Hooft and Veltman [31] (HV), which is more time consuming in computer calculations. However, the problem of defining chirality is a fundamental issue in every regularization scheme and not limited to dimensional regularization.

## 2.3 Renormalization

The simple  $\overline{\text{MS}}$  scheme is not always sufficient in practical calculations. Since it fixes only the divergent poles, it cannot describe the finite mixing of states with the same gauge quantum numbers. When making connection to physical quantities, additional renormalization conditions have to be specified.

To illustrate this characteristic of the  $\overline{\text{MS}}$  scheme, we work out the renormalization of the flavour-changing coupling of the photon  $A^\mu$  to the quark fields  $b$  and  $s$  in the following. This part of the Lagrangian is relevant for the calculation of the penguin diagrams in the processes  $B \rightarrow X_s\gamma$ ,  $B \rightarrow X_s$  gluon and  $B \rightarrow X_s\mu^+\mu^-$ .

The flavour-changing vertex  $\bar{s}A^\mu b$  is not present in the bare Lagrangian. The corresponding amplitude is therefore only renormalized by the mixing of the quark fields under radiative corrections to the self-energy. The flavour-conserving vertex is given by

$$\mathcal{L} = -\frac{1}{3}e^0\bar{d}_i^0\gamma_\mu d_i^0 A^{0,\mu}, \quad (2.15)$$

with the down-type quark fields  $d_i = d, s, b$ . The index “0” indicates that the fields and parameters are unrenormalized. The flavour-changing vertex is generated via the quark field-strength renormalization. The field-strength renormalization of the left-handed quark fields can be written to first order as

$$d_i^{L,0} = ((Z^{d,L})^{1/2})_{ij} d_j^L = \left(Z_{ij}^{d,L}\right)^{1/2} d_j^L = \left(\delta_{ij} + \frac{1}{2}\delta Z_{ij}^{d,L}\right) d_j^L. \quad (2.16)$$

The expression for the right-handed fields is analogous. The expression for the complex

conjugated fields is

$$\bar{d}_i^0 = \bar{d}_j \left( \delta_{ij} + \frac{1}{2} \delta Z_{ij}^{d,L*} \right). \quad (2.17)$$

Now we can write (2.15) in terms of renormalized fields. The flavour-changing part is given to one-loop order by

$$-\frac{1}{3} e \bar{d}^L \gamma_\mu \frac{1}{2} (\delta Z_{ji}^{d,L*} + \delta Z_{ij}^{d,L}) d_j^L A^\mu - \frac{1}{3} e \bar{d}^R \gamma_\mu \frac{1}{2} (\delta Z_{ji}^{d,R*} + \delta Z_{ij}^{d,R}) d_j^R A^\mu. \quad (2.18)$$

In order to determine  $\delta Z_{ij}^{d,L}$  and  $\delta Z_{ij}^{d,R}$ , we have to specify renormalization conditions on the quark self-energy, for which we will first derive a formal expression. Written in flavour eigenstates  $d_j^{0'}$ , the kinetic part of the Lagrangian reads

$$\mathcal{L} = \bar{d}_i^{0'} i \not{\partial} d_i^{0'} - \bar{d}_i^{0'} \mu_{d,ij}^0 d_j^{0'}, \quad (2.19)$$

where  $\mu_{d,ij}$  is the down-type mass matrix. The flavour eigenstates are transformed into mass eigenstates with a biunitary transformation that also yields the CKM matrix. The resulting Lagrangian is

$$\mathcal{L} = \bar{d}_i^0 i \not{\partial} d_i^0 - \bar{d}_i^0 M_{d,ij}^0 d_j^0, \quad (2.20)$$

with a diagonal mass matrix  $M_{d,ij}$ .

The mass renormalization is given by

$$M_{d,ii}^0 \equiv m_{d,i}^0 = Z_i^{d,m} m_{d,i}. \quad (2.21)$$

Note that we introduce only a flavour-diagonal mass renormalization constant  $Z_i^{d,m}$ , since the mass matrix of the bare fields is diagonal in (2.20). With the help of (2.16) and (2.21) we can write the Lagrangian (2.20) in terms of renormalized fields. In particular, the flavour-diagonal part of the mass counterterms is given by

$$-\bar{d}_i^L \left[ \delta Z_i^{d,m} + \frac{1}{2} \text{Re} \left\{ \delta Z_{ii}^{d,L} + \delta Z_{ii}^{d,R} \right\} - \frac{i}{2} \text{Im} \left\{ \delta Z_{ii}^{d,L} - \delta Z_{ii}^{d,R} \right\} \right] m_{d,i} d_i^R + \text{h.c.} \quad (2.22)$$

The last two terms in (2.22) are fixed by the field strength renormalization. The imaginary part of the field strength renormalization in the third term is needed for the absorptive part of the self-energy, while there are no contributions coming from the CKM matrix since it is unitary.

The unrenormalized self-energy can be written as

$$\Sigma_{ij}(\not{p}) = \Sigma_{ij}^L(p^2) \not{p} P_L + \Sigma_{ij}^R(p^2) \not{p} P_R + \Sigma_{ij}^l(p^2) P_L + \Sigma_{ij}^r(p^2) P_R, \quad (2.23)$$

with the chiral projectors  $P_{L/R} = (1 \mp \gamma_5)/2$ . In the SM as well as in the ACD model, the part independent of  $\not{p}$  can be written at one-loop order as

$$\Sigma_{ij}^l(p^2) P_L + \Sigma_{ij}^r(p^2) P_R = (m_{d,i} P_L + m_{d,j} P_R) \Sigma_{ij}^S(p^2), \quad (2.24)$$

with the function  $\Sigma_{ij}^S$  common to both the left-handed and the right-handed part.

As the next step we include the counterterms. The resulting renormalized self-energy reads

$$\begin{aligned}
\hat{\Sigma}_{ij}(\not{p}) &= \Sigma_{ij}(\not{p}) + \Sigma_{ij}^{\text{c.t.}}(\not{p}) \\
&= \left[ \Sigma_{ij}^L(p^2) - \frac{1}{2}(\delta Z_{ji}^{d,L*} + \delta Z_{ij}^{d,L}) \right] \not{p} P_L \\
&+ \left[ \Sigma_{ij}^R(p^2) - \frac{1}{2}(\delta Z_{ji}^{d,R*} + \delta Z_{ij}^{d,R}) \right] \not{p} P_R \\
&+ \left[ \delta_{ij} m_{d,i} \delta Z_i^{d,m} + \Sigma_{ij}^l(p^2) + \frac{1}{2} \left( \delta Z_{ij}^{d,R*} m_{d,j} + m_{d,i} \delta Z_{ij}^{d,L} \right) \right] P_L \\
&+ \left[ \delta_{ij} m_{d,i} \delta Z_i^{d,m} + \Sigma_{ij}^r(p^2) + \frac{1}{2} \left( \delta Z_{ij}^{d,L*} m_{d,j} + m_{d,i} \delta Z_{ij}^{d,R} \right) \right] P_R. \tag{2.25}
\end{aligned}$$

The renormalization condition that we exert on the self-energy is such that there is no flavor-changing propagation. However, since this requirement cannot be fulfilled in general for off-shell amplitudes, there is a certain ambiguity involved in the precise renormalization scheme. A common choice is the renormalization scheme by Denner [32]. For the inverse of the full propagator  $\hat{\Gamma}_{ij}$ , the following two conditions are imposed:

$$\widetilde{\text{Re}} \hat{\Gamma}_{ij}(\not{p}) d_j(p) = 0, \tag{2.26a}$$

$$\lim_{\not{p} \rightarrow m_{d,i}} \frac{i}{\not{p} - m_{d,i}} \widetilde{\text{Re}} \hat{\Gamma}_{ii}(\not{p}) d_i(p) = d_i(p), \tag{2.26b}$$

along with their hermitian conjugates, which we do not show here. The first expression fixes the positions of the poles in the propagator, whereas the second condition fixes the residues. Here  $\widetilde{\text{Re}}$  takes only the real part of the loop integrals appearing in the self-energy but not of the elements of the CKM matrix. Since the renormalized Lagrangian should be hermitian, the counterterms can only affect the non-absorptive parts.

The inverse of the full propagator is related to the self-energy (1-PI function)  $-i\hat{\Sigma}_{ij}(\not{p})$  by the identity

$$\hat{\Gamma}_{ij}(\not{p}) = -i(\not{p} - m_{d,i})\delta_{ij} + i\hat{\Sigma}_{ij}(\not{p}). \tag{2.27}$$

The conditions (2.26a) and (2.26b) translate readily into

$$\widetilde{\text{Re}} i\hat{\Sigma}_{ij}(\not{p}) d_j(p) = 0, \tag{2.28a}$$

$$\lim_{\not{p} \rightarrow m_{d,i}} \frac{i}{\not{p} - m_{d,i}} \widetilde{\text{Re}} i\hat{\Sigma}_{ii}(\not{p}) d_i(p) = d_i(p). \tag{2.28b}$$

Of these, we only need the first condition (2.28a) that fixes the off-diagonal part of the self-energy. For the special case  $d_i = s, d_j = b$  we can set  $m_s = 0$  and use

$$\Sigma_{sb}^l(p^2) \sim m_s, \quad \Sigma_{sb}^R(p^2) \sim m_s. \quad (2.29)$$

Applying (2.28a) and its conjugate to (2.25) now yields the four conditions

$$\delta Z_{sb}^{d,R} = 0, \quad (2.30a)$$

$$\delta Z_{bs}^{d,R*} = 0, \quad (2.30b)$$

$$m_b \widetilde{\text{Re}} i \Sigma_{sb}^L(m_b^2) + \widetilde{\text{Re}} i \Sigma_{sb}^r(m_b^2) - \frac{i}{2} m_b \delta Z_{sb}^{d,L} = 0, \quad (2.30c)$$

$$\widetilde{\text{Re}} i \Sigma^r sb(0) + \frac{i}{2} m_b \delta Z_{bs}^{d,L*} = 0. \quad (2.30d)$$

These conditions completely specify the counterterm vertex (2.18) to be

$$\mathcal{L}_{b \rightarrow s\gamma, \text{c.t.}} = -\frac{1}{3} e \widetilde{\text{Re}} (\Sigma_{sb}^L(m_b^2) + m_b^{-1} \Sigma_{sb}^r(m_b^2) - m_b^{-1} \Sigma_{sb}^r(0)) \bar{s} \gamma_\mu P_L b A^\mu. \quad (2.31)$$

It should be emphasized that the structure of this counterterm depends on the renormalization conditions. In the renormalization scheme proposed by Gambino, Grassi and Madricardo [33], the counterterm is given by

$$\mathcal{L}_{b \rightarrow s\gamma, \text{c.t.}} = -\frac{1}{3} e \Sigma_{sb}^L(0) \bar{s} \gamma_\mu P_L b A^\mu. \quad (2.32)$$

Of course, all physical observables are independent of the renormalization scheme.

## 2.4 The Renormalization Group

The values of the renormalized parameters do not only depend on the values of their bare counterparts but also on the renormalization scheme and the renormalization scale. In a cut-off regularization this scale would be given by the cut-off scale  $\Lambda_0$ . In dimensional regularization we have introduced the scale  $\mu$  in (2.11). In the following, we only discuss the  $\overline{\text{MS}}$  scheme in dimensional regularization.

Due to the occurrence of large logarithms in the loop calculations, the renormalization scale must correspond to the typical masses and momenta of particles involved. In the  $\overline{\text{MS}}$  scheme, heavy particles do not decouple automatically and therefore have to be integrated out explicitly. In this process a low-energy theory without the heavy particles is matched to the full theory at the scale of the heavy particles. The couplings of the parameters and



operators in the new Lagrangian are then evolved down to a lower scale with the help of the renormalization group (RG). This lower scale is given by the masses and momenta of the external particles involved in the processes we are interested in.

An infinitesimal change in  $\mu$  will result in a shift of the renormalized parameters of the Lagrangian. The differential equations that describe this change are called renormalization group equations (RGEs). For the coupling constant in QCD we have

$$\mu \frac{dg}{d\mu} = \beta(g(\mu, \varepsilon)), \quad (2.33)$$

where the function  $\beta$  is given by

$$\beta(g(\mu, \varepsilon)) = -\varepsilon g - g\mu \frac{dZ_g}{d\mu} \frac{1}{Z_g} \quad (2.34)$$

with the renormalization constant  $Z_g$  defined by

$$g_0 = Z_g g \mu^\varepsilon \quad (2.35)$$

and

$$\beta(g(\mu), \varepsilon) = -\varepsilon g + \beta(g). \quad (2.36)$$

We have already mentioned that in the  $\overline{\text{MS}}$  scheme, the renormalization group function  $\beta(g)$  depends only on  $g$  but not explicitly on  $\mu$ . The function  $\beta(g)$  can therefore be written as

$$\beta(g) = -\beta_0 \frac{g^3}{16\pi^2} - \beta_1 \frac{g^5}{(16\pi^2)^2} + \mathcal{O}(g^7). \quad (2.37)$$

The generalization to theories with more complicated gauge groups like the Standard Model gauge group  $SU(3)_c \times SU(2)_L \times U(1)_Y$  is obvious. The leading order solution for the RGE of the  $SU(3)_c$  (QCD) coupling constant reads

$$\alpha_s(\mu) = \frac{\alpha_s(\mu_0)}{1 - \beta_0 \alpha_s(\mu_0) \log(\mu_0/\mu)/2\pi}, \quad (2.38)$$

with the leading order coefficient of the  $\beta$ -function

$$\beta_0 = \frac{11N - 2f}{3} \quad (2.39)$$

depending on the number of colours  $N$  ( $N = 3$  for QCD) and the number of quark flavours  $f$ . Similar formulae can be derived for the anomalous dimensions of the masses and field strengths of the quark fields

$$\gamma_m = Z_m^{-1} \mu \frac{dZ_m}{d\mu}, \quad \gamma_\psi^{-1} = \mu \frac{dZ_\psi}{d\mu}. \quad (2.40)$$



# Chapter 3

## Flavour physics

## 3.1 Penguin Diagrams in the ACD Model

### 3.1.1 Effective vertices

The rare decays in the ACD model we consider in this thesis are governed as in the SM by various penguin diagrams. The SM contributions to the  $\Delta F = 1$  box diagrams are subleading but have to be included in the analysis. On the other hand the KK contributions to the box diagrams are tiny [3] and can be neglected.

The penguin vertices including electroweak counterterms can be conveniently expressed in terms of the functions  $C, D, E, D'$  and  $E'$  which correspond to  $Z^0$  penguins,  $\gamma$  penguins, gluon penguins,  $\gamma$ -magnetic penguins and chromomagnetic penguins, respectively. In the 't Hooft–Feynman gauge for the  $W^\pm$  and  $G^\pm$  propagators they are given as:

$$\bar{s}Zd = i\lambda_t \frac{G_F}{\sqrt{2}} \frac{g_2}{2\pi^2} \frac{M_W^2}{\cos\theta_w} C(x_t, 1/R) \bar{s}\gamma_\mu(1 - \gamma_5)d, \quad (3.1)$$

$$\bar{s}\gamma d = -i\lambda_t \frac{G_F}{\sqrt{2}} \frac{e}{8\pi^2} D(x_t, 1/R) \bar{s}(q^2\gamma_\mu - q_\mu \not{q})(1 - \gamma_5)d, \quad (3.2)$$

$$\bar{s}G^a d = -i\lambda_t \frac{G_F}{\sqrt{2}} \frac{g_s}{8\pi^2} E(x_t, 1/R) \bar{s}_\alpha(q^2\gamma_\mu - q_\mu \not{q})(1 - \gamma_5)T_{\alpha\beta}^a d_\beta, \quad (3.3)$$

$$\bar{s}\gamma' b = i\bar{\lambda}_t \frac{G_F}{\sqrt{2}} \frac{e}{8\pi^2} D'(x_t, 1/R) \bar{s}[i\sigma_{\mu\lambda}q^\lambda[m_b(1 + \gamma_5)]]b, \quad (3.4)$$

$$\bar{s}G'^a b = i\bar{\lambda}_t \frac{G_F}{\sqrt{2}} \frac{g_s}{8\pi^2} E'(x_t, 1/R) \bar{s}_\alpha[i\sigma_{\mu\lambda}q^\lambda[m_b(1 + \gamma_5)]]T_{\alpha\beta}^a b_\beta, \quad (3.5)$$

where  $G_F$  is the Fermi constant,  $\theta_w$  is the weak mixing angle and the CKM factors are

$$\lambda_t = V_{ts}^* V_{td}, \quad \bar{\lambda}_t = V_{ts}^* V_{tb}. \quad (3.6)$$

In these vertices  $q_\mu$  is the *outgoing* gluon or photon momentum and  $T^a$  are QCD colour matrices. The last two vertices involve an on-shell photon and gluon, respectively. We have set  $m_s = 0$  in the above vertices.

Each function in (3.1)-(3.5) possesses the structure

$$F(x_t, 1/R) = F_0(x_t) + \sum_{n=1}^{\infty} F_n(x_t, x_n), \quad F = C, D, E, D', E', \quad (3.7)$$

with

$$x_n = \frac{m_n^2}{M_W^2}, \quad m_n = \frac{n}{R}. \quad (3.8)$$

The functions  $F_n(x_t, x_n)$  in (3.7) are defined through

$$F_n(x_t, x_n) = G(x_{t(n)}) - G(x_{u(n)}), \quad (3.9)$$

with

$$x_{i(n)} = m_0^2 + \frac{n^2}{R^2}. \quad (3.10)$$

Here  $m_0$  is the zero-mode mass, as  $M_W$ ,  $M_Z$ ,  $m_t$ . The functions  $G(x_{t(n)})$  and  $G(x_{u(n)})$  represent the contributions of the  $\mathcal{Q}_{t(n)}$ ,  $\mathcal{U}_{t(n)}$  and  $\mathcal{Q}_{u(n)}$ ,  $\mathcal{U}_{u(n)}$  modes, respectively.

The functions  $F_0(x_t)$  result from SM penguin diagrams, whereas the sum represents the KK contributions. The penguin diagrams in the SM were calculated by various authors, in particular by Inami and Lim [34]:

$$C_0(x_t) = \frac{x_t}{8} \left[ \frac{x_t - 6}{x_t - 1} + \frac{3x_t + 2}{(x_t - 1)^2} \ln x_t \right], \quad (3.11)$$

$$D_0(x_t) = -\frac{4}{9} \ln x_t + \frac{-19x_t^3 + 25x_t^2}{36(x_t - 1)^3} + \frac{x_t^2(5x_t^2 - 2x_t - 6)}{18(x_t - 1)^4} \ln x_t, \quad (3.12)$$

$$E_0(x_t) = -\frac{2}{3} \ln x_t + \frac{x_t^2(15 - 16x_t + 4x_t^2)}{6(1 - x_t)^4} \ln x_t + \frac{x_t(18 - 11x_t - x_t^2)}{12(1 - x_t)^3}, \quad (3.13)$$

$$D'_0(x_t) = -\frac{(8x_t^3 + 5x_t^2 - 7x_t)}{12(1 - x_t)^3} + \frac{x_t^2(2 - 3x_t)}{2(1 - x_t)^4} \ln x_t, \quad (3.14)$$

$$E'_0(x_t) = -\frac{x_t(x_t^2 - 5x_t - 2)}{4(1 - x_t)^3} + \frac{3}{2} \frac{x_t^2}{(1 - x_t)^4} \ln x_t. \quad (3.15)$$

The  $Z^0$  penguin functions  $C_n(x_t, x_n)$  have been calculated in [3]:

$$C_n(x_t, x_n) = \frac{x_t}{8(x_t - 1)^2} \left[ x_t^2 - 8x_t + 7 + (3 + 3x_t + 7x_n - x_t x_n) \ln \frac{x_t + x_n}{1 + x_n} \right]. \quad (3.16)$$

In this thesis we calculate the remaining functions  $D_n(x_t, x_n)$ ,  $E_n(x_t, x_n)$ ,  $D'_n(x_t, x_n)$  and  $E'_n(x_t, x_n)$ .

### 3.1.2 General Structure of the Calculation

The function  $F_n(x_t, x_n)$  with  $F = D, E, D', E'$  are found by calculating the vertex diagrams in Fig. 3.1. Contrary to the  $Z^0$  penguins where one has to add an electroweak counterterm as discussed in [35], this is not necessary for the  $\gamma$  and gluon penguins. Here the counterterms are only formally used to render zero the coefficients of the dimension 4 operators  $\bar{s}A_{PL}q$  and  $\bar{s}\mathbf{T}^a\mathcal{G}^a_{PL}q$  with  $q = d, b$ . This is a consequence of gauge invariance when the quark fields are set on-shell with the renormalization condition given in [32].

In contrast to the calculation of the  $Z^0$ -vertex the external momenta in Fig. 3.1 and the masses of external quarks cannot be neglected.

The effective Hamiltonian at the matching scale  $\mu_W$  reads

$$\mathcal{H}_{\text{eff}}(b \rightarrow s\gamma, G) = -\frac{G_F}{\sqrt{2}} V_{ts}^* V_{tb} \left[ \sum_{i=30}^{36} C_i(\mu_W) Q_i + C_{7\gamma}(\mu_W) Q_{7\gamma} + C_{8G}(\mu_W) Q_{8G} \right], \quad (3.17)$$

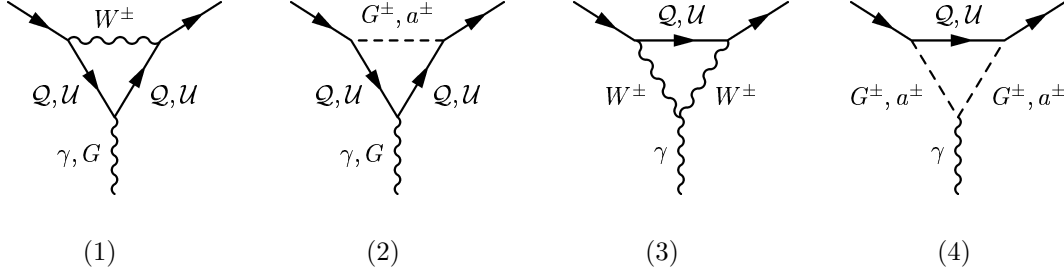


Figure 3.1: Penguin diagrams contributing to  $F_n(x_t, x_n)$ . The external gauge bosons are background fields.

with the operators [36]

$$Q_{7\gamma} = \frac{e}{4\pi^2} m_b (\bar{s} \sigma_{\mu\nu} P_R b) F^{\mu\nu}, \quad (3.18)$$

$$Q_{8G} = \frac{g_s}{4\pi^2} m_b (\bar{s} \sigma_{\mu\nu} P_R \mathbf{T}^a b) G^{a,\mu\nu}, \quad (3.19)$$

$$Q_{30} = \frac{i}{4\pi^2} M_W^2 (\bar{s} \not{D} P_L b), \quad (3.20)$$

$$Q_{31} = \frac{g_s}{4\pi^2} (\bar{s} P_R \gamma_\mu \mathbf{T}^a b) D_\nu G^{a,\mu\nu} + Q_4, \quad (3.21)$$

$$Q_{32} = \frac{1}{4\pi^2} m_b (\bar{s} P_R \not{D} \not{D} b), \quad (3.22)$$

$$Q_{33} = \frac{i}{4\pi^2} (\bar{s} P_R \not{D} \not{D} \not{D} b), \quad (3.23)$$

$$Q_{34} = \frac{ig_s}{4\pi^2} \bar{s} P_R \left[ \overleftarrow{\not{D}} \sigma_{\mu\nu} \mathbf{T}^a - \mathbf{T}^a \sigma_{\mu\nu} (\not{D} + im_b) \right] b G^{a,\mu\nu}, \quad (3.24)$$

$$Q_{35} = \frac{ie}{4\pi^2} \bar{s} P_R \left[ \overleftarrow{\not{D}} \sigma_{\mu\nu} - \sigma_{\mu\nu} (\not{D} + im_b) \right] b F^{\mu\nu}, \quad (3.25)$$

$$Q_{36} = \frac{e}{4\pi^2} (\bar{s} P_R \gamma_\mu b) \partial_\nu F^{\mu\nu} - Q_9. \quad (3.26)$$

The covariant derivative in the effective Lagrangian is defined as<sup>1</sup>

$$D_\mu \psi = (\partial_\mu + ieQ_\psi A_\mu + ig_s \mathbf{T}^a G_\mu^a) \psi. \quad (3.27)$$

In the operators  $Q_{34}$  and  $Q_{35}$  it acts only on the spinors, but not on the field strength tensors  $F^{\mu\nu}$  and  $G^{a,\mu\nu}$ .

In this off-shell operator basis we have omitted the four-quark operators as they are not relevant for the calculation of the functions  $F$ . They can be found in [36], in particular the operators  $Q_4$  and  $Q_9$  that appear in the definition of  $Q_{31}$  and  $Q_{36}$ . The effective vertices (3.2)-(3.5) correspond to the operators  $Q_{36}$ ,  $Q_{31}$ ,  $Q_{7\gamma}$  and  $Q_{8G}$ , respectively.

<sup>1</sup>On the effective side we use a different sign convention for the couplings  $e$  and  $g_s$  compared to the Feynman rules in this thesis and in [3].

In the calculation of the functions  $F$  we used the off-shell amplitude for the matching, i.e. no equations of motion are applied. In order to maintain gauge invariance the method of background fields [37] is used, see Appendix A. Consequently the matching is done with the full set of operators (3.18)-(3.26). For the derivation of the Feynman rules of the ACD model in the background field method, we developed a suitable computer program using Mathematica [38].

For the full side the diagrams (1)-(4) in Fig. 3.1 were evaluated in 't Hooft-Feynman gauge with the Feynman rules given in Appendix B.

The effective side can be directly matched to the full side. Comparing (3.2)-(3.5) with (3.17) we can read off

$$D = -C_{36}^{(0)}(\mu_W), \quad D' = -2C_{7\gamma}^{(0)}(\mu_W), \quad (3.28)$$

$$E = -C_{31}^{(0)}(\mu_W), \quad E' = -2C_{8G}^{(0)}(\mu_W), \quad (3.29)$$

where “(0)” indicates the leading coefficients without QCD corrections.

The functions  $F$  can also be determined in an on-shell calculation where the equations of motion for the quark fields and the relation  $q^2 = 0$  are applied [6, 39].

### 3.1.3 The functions $D, E, D', E'$ and $Z$

For the evaluation of the diagrams of Fig. 3.1 we also wrote a computer program in Mathematica. We find

$$\begin{aligned} & D_n(x_t, x_n) \\ &= \frac{x_t(35 + 8x_t - 19x_t^2 + 6x_n^2(10 - 9x_t + 3x_t^2) + 3x_n(53 - 58x_t + 21x_t^2))}{108(x_t - 1)^3} \\ &+ \frac{1}{6}(4 - 2x_n + 4x_n^2 + x_n^3) \ln \frac{x_n}{1 + x_n} \\ &- \frac{1}{18(x_t - 1)^4} \left[ 12 - 38x_t + 54x_t^2 - 27x_t^3 + 3x_t^4 + x_n^3(3 + x_t) \right. \\ &\left. + 3x_n^2(4 - x_t + x_t^2) + x_n(-6 + 42x_t - 33x_t^2 + 9x_t^3) \right] \ln \frac{x_n + x_t}{1 + x_n}, \end{aligned} \quad (3.30)$$

$$\begin{aligned} & E_n(x_t, x_n) \\ &= -\frac{x_t(35 + 8x_t - 19x_t^2 + 6x_n^2(10 - 9x_t + 3x_t^2) + 3x_n(53 - 58x_t + 21x_t^2))}{36(x_t - 1)^3} \\ &- \frac{1}{2}(1 + x_n)(-2 + 3x_n + x_n^2) \ln \frac{x_n}{1 + x_n} \\ &+ \frac{(1 + x_n)(-6 + 19x_t - 9x_t^2 + x_n^2(3 + x_t) + x_n(9 - 4x_t + 3x_t^2))}{6(x_t - 1)^4} \ln \frac{x_n + x_t}{1 + x_n}, \end{aligned} \quad (3.31)$$

$$\begin{aligned}
& D'_n(x_t, x_n) \\
&= \frac{x_t(-37 + 44x_t + 17x_t^2 + 6x_n^2(10 - 9x_t + 3x_t^2) - 3x_n(21 - 54x_t + 17x_t^2))}{36(-1 + x_t)^3} \\
&+ \frac{x_n(2 - 7x_n + 3x_n^2)}{6} \ln \frac{x_n}{1 + x_n} \\
&- \frac{(-2 + x_n + 3x_t)(x_t + 3x_t^2 + x_n^2(3 + x_t) - x_n(1 + (-10 + x_t)x_t))}{6(-1 + x_t)^4} \\
&\times \ln \frac{x_n + x_t}{1 + x_t}, \tag{3.32}
\end{aligned}$$

$$\begin{aligned}
& E'_n(x_t, x_n) \\
&= \frac{x_t(-17 - 8x_t + x_t^2 - 3x_n(21 - 6x_t + x_t^2) - 6x_n^2(10 - 9x_t + 3x_t^2))}{12(x_t - 1)^3} \\
&- \frac{1}{2}x_n(1 + x_n)(-1 + 3x_n) \ln \frac{x_n}{1 + x_n} \\
&+ \frac{(1 + x_n)(x_t + 3x_t^2 + x_n^2(3 + x_t) - x_n(1 + (-10 + x_t)x_t))}{2(x_t - 1)^4} \ln \frac{x_n + x_t}{1 + x_n}. \tag{3.33}
\end{aligned}$$

In Figs. 3.2 - 3.5 we show the dependence of the functions  $F(x_t, 1/R)$  on  $1/R$ . The constant dashed lines are the SM values. Due to a partial cancellation of two contributions, the impact of the KK modes on the function  $D$  is negligible. The function  $E$  is moderately enhanced but this enhancement plays only a marginal role in our phenomenological applications. Most interesting are the very strong suppressions of  $D'$  (36%) and  $E'$  (66%) relative to the SM values for  $1/R = 300$  GeV.

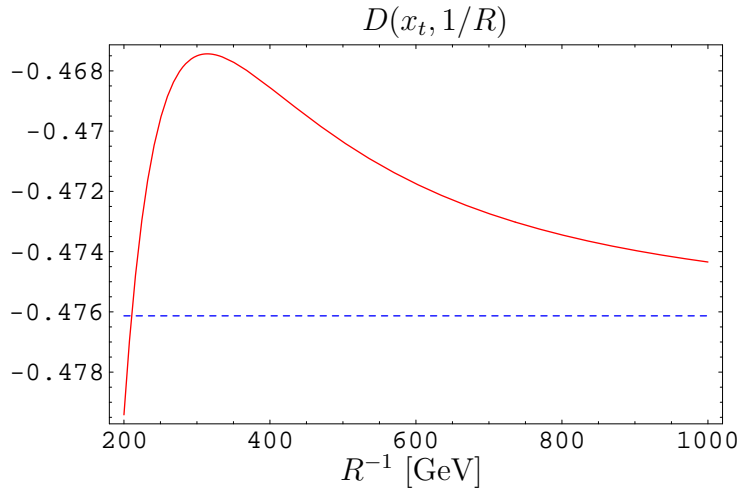
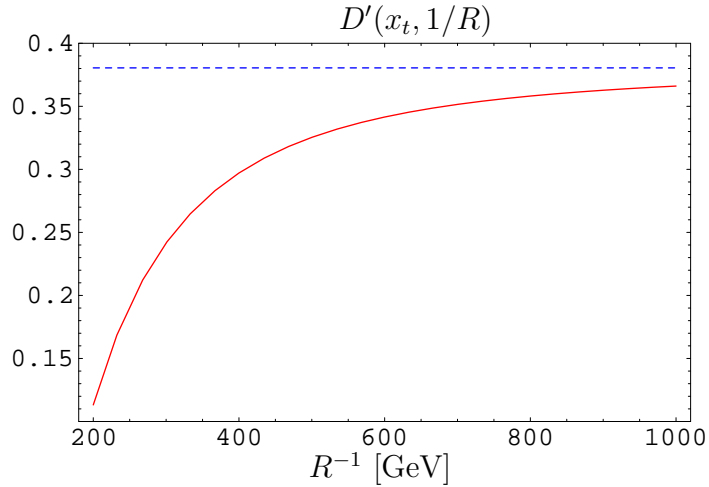
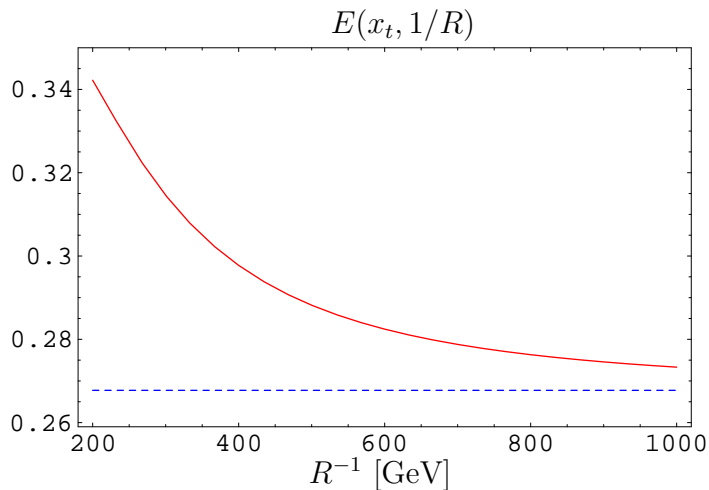


Figure 3.2: The functions  $D(x_t, 1/R)$  and  $D_0(x_t)$ .



Figure 3.3: The functions  $D'(x_t, 1/R)$  and  $D'_0(x_t)$ .Figure 3.4: The functions  $E(x_t, 1/R)$  and  $E_0(x_t)$ .

While the penguin functions  $E$ ,  $D'$  and  $E'$  are gauge independent, this is not the case for  $C$ ,  $D$  and the  $\Delta F = 1$  box functions  $B^{\nu\bar{\nu}}$  and  $B^{\mu\bar{\mu}}$  considered in [3]. They can be combined to the gauge independent functions [40]

$$X(x_t, 1/R) = C(x_t, 1/R) + B^{\nu\bar{\nu}}(x_t, 1/R) = X_0(x_t) + \Delta X, \quad (3.34)$$

$$Y(x_t, 1/R) = C(x_t, 1/R) + B^{\mu\bar{\mu}}(x_t, 1/R) = Y_0(x_t) + \Delta Y, \quad (3.35)$$

$$Z(x_t, 1/R) = C(x_t, 1/R) + \frac{1}{4}D(x_t, 1/R) = Z_0(x_t) + \Delta Z, \quad (3.36)$$

with  $\Delta X$ ,  $\Delta Y$  and  $\Delta Z$  representing the corrections due to KK modes. The SM contri-

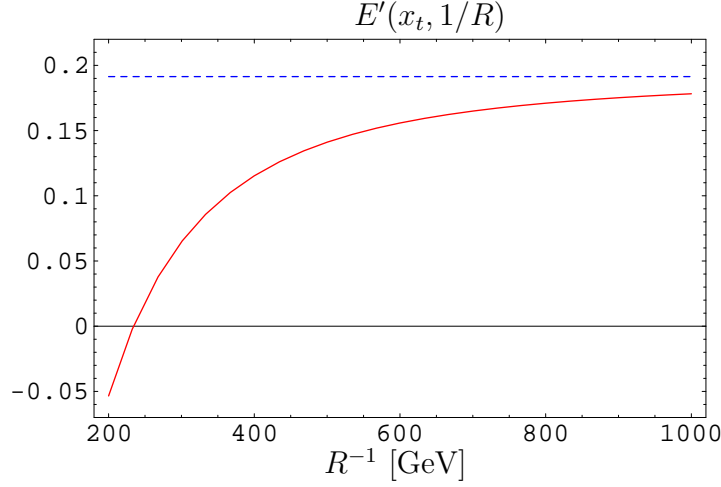


Figure 3.5: The functions  $E'(x_t, 1/R)$  and  $E'_0(x_t)$ .

butions are given as follows ( $m_t = 167$  GeV):

$$X_0(x_t) = \frac{x_t}{8} \left[ \frac{x_t + 2}{x_t - 1} + \frac{3x_t - 6}{(x_t - 1)^2} \ln x_t \right] = 1.526, \quad (3.37)$$

$$Y_0(x_t) = \frac{x_t}{8} \left[ \frac{x_t - 4}{x_t - 1} + \frac{3x_t}{(x_t - 1)^2} \ln x_t \right] = 0.980, \quad (3.38)$$

$$Z_0(x_t) = -\frac{1}{9} \ln x_t + \frac{18x_t^4 - 163x_t^3 + 259x_t^2 - 108x_t}{144(x_t - 1)^3} + \frac{32x_t^4 - 38x_t^3 - 15x_t^2 + 18x_t}{72(x_t - 1)^4} \ln x_t = 0.679. \quad (3.39)$$

The KK contributions to the functions  $B^{\nu\bar{\nu}}$ ,  $B^{\mu\bar{\mu}}$  [3] and to the function D found here are negligible. The corrections to the functions X, Y and Z are therefore given by

$$\Delta X = \Delta Y = \Delta Z = \sum_{n=1}^{\infty} C_n(x_t, x_n) \quad (3.40)$$

to an excellent approximation.

In Table 3.1 we give the values of the functions X, Y C calculated in [3] and of Z, D E, D', E' calculated here for different values of  $1/R$  and  $m_t = 167$  GeV. For  $1/R = 300$  GeV, the functions X, Y, Z are enhanced by 10%, 15% and 23% relative to the SM values, respectively. These enhancements are smaller than the corresponding suppressions of D' and E', but sizable additive QCD corrections will soften the effect of the latter suppressions in the branching ratios considered here.

$1/R$ [GeV]	$X$	$Y$	$Z$	$E$	$D'$	$E'$	$C$	$D$
200	1.826	1.281	0.990	0.342	0.113	-0.053	1.099	-0.479
250	1.731	1.185	0.893	0.327	0.191	0.019	1.003	-0.470
300	1.674	1.128	0.835	0.315	0.242	0.065	0.946	-0.468
400	1.613	1.067	0.771	0.298	0.297	0.115	0.885	-0.469
SM	1.526	0.980	0.679	0.268	0.380	0.191	0.798	-0.476

Table 3.1: Values for the functions  $X$ ,  $Y$ ,  $Z$ ,  $E$ ,  $D'$ ,  $E'$ ,  $C$  and  $D$ . The gauge dependent functions  $C$  and  $D$  are given in 't Hooft-Feynman gauge.

## 3.2 The decays $B \rightarrow X_s \gamma$ and $B \rightarrow X_s$ gluon

### 3.2.1 Effective Hamiltonian

We will first present the LO analysis of the decays where the impact of the KK modes can be seen most clearly. The effective Hamiltonian for the decays  $B \rightarrow X_s \gamma$  and  $B \rightarrow X_s$  gluon is given by

$$\mathcal{H}_{\text{eff}}(b \rightarrow s\gamma) = -\frac{G_F}{\sqrt{2}} V_{ts}^* V_{tb} \left[ \sum_{i=1}^6 C_i(\mu_b) Q_i + C_{7\gamma}(\mu_b) Q_{7\gamma} + C_{8G}(\mu_b) Q_{8G} \right]. \quad (3.41)$$

Here we have neglected the term proportional to  $V_{us}^* V_{ub}$  which is suppressed relative to  $V_{ts}^* V_{tb}$  in view of  $|V_{us}^* V_{ub}/V_{ts}^* V_{tb}| < 0.02$ . The explicit form of the four-quark operators can be found in [42]. The magnetic penguin operators  $Q_{7\gamma}$  and  $Q_{8G}$  are given in (3.18).

The matching calculation is performed at the scale  $\mu_W = \mathcal{O}(M_W)$ , yielding the Wilson coefficients

$$C_2^{(0)}(\mu_W) = 1, \quad C_{7\gamma}^{(0)}(\mu_W) = -\frac{1}{2} D'(x_t, 1/R), \quad C_{8G}^{(0)}(\mu_W) = -\frac{1}{2} E'(x_t, 1/R). \quad (3.42)$$

At this scale, all other coefficients are zero. However, at NLO they generally obtain non-zero values through the renormalization group running to the scale  $\mu_b = 5$  GeV.

In order to keep the LO Wilson coefficients renormalization scheme independent [43], we also introduce the effective coefficients  $C_{7\gamma}^{(0)\text{eff}}$  and  $C_{8G}^{(0)\text{eff}}$ . Using the formulae in [43] we get

$$C_{7\gamma}^{(0)\text{eff}}(\mu_b) = \eta^{\frac{16}{23}} C_{7\gamma}^{(0)}(\mu_W) + \frac{8}{3} \left( \eta^{\frac{14}{23}} - \eta^{\frac{16}{23}} \right) C_{8G}^{(0)}(\mu_W) + C_2^{(0)}(\mu_W) \sum_{i=1}^8 h_i \eta^{a_i}, \quad (3.43)$$

$$C_{8G}^{(0)\text{eff}}(\mu_b) = \eta^{\frac{14}{23}} C_{8G}^{(0)}(\mu_W) + C_2^{(0)}(\mu_W) \sum_{i=1}^8 \bar{h}_i \eta^{a_i}, \quad (3.44)$$

with  $\eta = \alpha_s(\mu_W)/\alpha_s(\mu_b)$ . The superscript “0” indicates the LO approximation. The values of  $a_i$ ,  $h_i$  and  $\bar{h}_i$  are given in Table 3.2. The resulting LO values of the Wilson coefficients  $C_{7\gamma}^{(0)\text{eff}}(\mu_b)$  and  $C_{8G}^{(0)\text{eff}}(\mu_b)$  can be found in Table 3.3.

$i$	1	2	3	4	5	6	7	8
$a_i$	$\frac{14}{23}$	$\frac{16}{23}$	$\frac{6}{23}$	$-\frac{12}{23}$	0.4086	-0.4230	-0.8994	0.1456
$h_i$	2.2996	-1.0880	$-\frac{3}{7}$	$-\frac{1}{14}$	-0.6494	-0.0380	-0.0185	-0.0057
$\bar{h}_i$	0.8623	0	0	0	-0.9135	0.0873	-0.0571	0.0209

Table 3.2: Magic Numbers.

	$\mu_b = 2.5 \text{ GeV}$		$\mu_b = 5.0 \text{ GeV}$		$\mu_b = 7.5 \text{ GeV}$	
$1/R [\text{GeV}]$	$C_{7\gamma}^{(0)\text{eff}}$	$C_{8G}^{(0)\text{eff}}$	$C_{7\gamma}^{(0)\text{eff}}$	$C_{8G}^{(0)\text{eff}}$	$C_{7\gamma}^{(0)\text{eff}}$	$C_{8G}^{(0)\text{eff}}$
200	-0.236	-0.076	-0.192	-0.053	-0.169	-0.040
250	-0.264	-0.100	-0.223	-0.079	-0.201	-0.068
300	-0.282	-0.114	-0.242	-0.096	-0.221	-0.086
400	-0.301	-0.131	-0.264	-0.114	-0.244	-0.105
SM	-0.331	-0.156	-0.296	-0.142	-0.278	-0.135

Table 3.3: Wilson coefficients  $C_{7\gamma}^{(0)\text{eff}}$  and  $C_{8G}^{(0)\text{eff}}$  in LO for  $m_t = 167 \text{ GeV}$  as functions of  $1/R$  and various values of  $\mu_b$ .

Two lessons can be learnt from these results. First, the impact of the KK modes on the coefficients  $C_{7\gamma}^{(0)\text{eff}}(\mu_b)$  and  $C_{8G}^{(0)\text{eff}}(\mu_b)$  is substantially smaller than on  $C_{7\gamma}^{(0)}(\mu_W)$  and  $C_{8G}^{(0)}(\mu_W)$  in (3.42). This is due to the large QCD correction in the last term in (3.43) and (3.44), respectively. This correction, which is also responsible for the large QCD enhancement of  $B \rightarrow X_s \gamma$  and  $B \rightarrow X_s$  gluon [44, 45] screens considerably the effects of the KK modes. For the values  $m_t = 167 \text{ GeV}$ ,  $1/R = 300 \text{ GeV}$ ,  $\mu_b = 5 \text{ GeV}$  and  $\alpha_s^{(5)}(M_Z) = 0.118$ , we find

$$\begin{aligned} C_{7\gamma}^{(0)\text{eff}}(\mu_b) &= 0.695 C_{7\gamma}^{(0)}(\mu_W) + 0.085 C_{8G}^{(0)}(\mu_W) - 0.158 C_2^{(0)}(\mu_W) \\ &= 0.695 (-0.121) + 0.085 (-0.033) - 0.158 = -0.245 \end{aligned} \quad (3.45)$$

and

$$\begin{aligned} C_{8G}^{(0)\text{eff}}(\mu_b) &= 0.727 C_{8G}^{(0)}(\mu_W) - 0.074 C_2^{(0)}(\mu_W) \\ &= 0.727 (-0.033) - 0.074 = -0.098, \end{aligned} \quad (3.46)$$

to be compared with the SM values  $-0.300$  and  $-0.144$ , respectively.

The second observation we make is the large  $\mu_b$ -dependence of the coefficients. This LO scale uncertainty is substantially reduced when including NLO corrections which we have to do for a phenomenologically viable analysis. For the SM these corrections are well known. For scales  $\mu < 1/R$  there are no KK excitations present, hence the only unknown NLO part are the ACD corrections to the Inami-Lim functions  $D'$  and  $E'$ . Since these are of order  $\mathcal{O}(\alpha_s)$  and further suppressed by the high masses of order  $\mathcal{O}(1/R)$ , we can neglect them to a good approximation.

### 3.2.2 Branching Ratio for $B \rightarrow X_s \gamma$

In our analysis we used the experimental world average resulting for the decay  $B \rightarrow X_s \gamma$  from the data by CLEO, ALEPH, BABAR and BELLE [46]

$$Br(B \rightarrow X_s \gamma)_{E_\gamma > 1.6 \text{ GeV}} = (3.28_{-0.36}^{+0.41}) \cdot 10^{-4}. \quad (3.47)$$

A more recent value [47]

$$Br(B \rightarrow X_s \gamma)_{E_\gamma > 250 \text{ MeV}} = (3.39_{-0.27}^{+0.30}) \cdot 10^{-4} \quad (3.48)$$

is given for a photon spectrum extrapolated down to  $E_\gamma > 250 \text{ MeV}$ . It implies only a minor change of (3.47), while the uncertainties are somewhat reduced, leading to essentially the same results.

The SM prediction [48, 49] is

$$Br(B \rightarrow X_s \gamma)_{E_\gamma > 1.6 \text{ GeV}}^{\text{SM}} = (3.57 \pm 0.30) \cdot 10^{-4} \quad (3.49)$$

which is consistent with the experimental value.

The LO approximation of the branching ratio is given by

$$\frac{Br(B \rightarrow X_s \gamma)}{Br(B \rightarrow X_c e \bar{\nu}_e)} = \frac{|V_{ts}^* V_{tb}|^2}{|V_{cb}|^2} \frac{6\alpha}{\pi f(z)} |C_7^{(0)\text{eff}}(\mu_b)|^2, \quad (3.50)$$

where  $f(z)$  with  $z = m_c/m_b$  is the phase space factor in  $Br(B \rightarrow X_c e \bar{\nu}_e)$ .

The corresponding NLO formulae that include also higher order electroweak effects [50] are complicated and can be found in [48]. As reviewed in [51, 52, 53], many groups contributed to obtain these NLO results. In our numerical NLO analysis we benefited enormously from the computer programs of the authors of [48, 50].

In Fig. 3.6 we can clearly see the strong suppression of the branching ratio by the KK modes. The shaded region represents the data in (3.47) and the upper (lower) dashed horizontal lines are the central values in the SM for  $m_c/m_b = 0.22$  ( $m_c/m_b = 0.29$ ). The solid lines represent the corresponding central values in the ACD model. The theoretical errors, not shown in the plot, are roughly  $\pm 10\%$  for all curves.

The theoretical prediction for  $Br(B \rightarrow X_s \gamma)$  depends sizably on the ratio  $m_c/m_b$ , which is the main uncertainty at NLO level. Since the charm mass enters the calculation first at NLO level, its renormalization ambiguity can only be resolved at the NNLO level. For the results in Table 3.4, we used  $m_c/m_b = 0.22$  in accordance with the arguments put forward in [48]. As seen in Fig. 3.6, for a value  $m_c/m_b = 0.29$  that has been used in the past, the branching ratio is smaller by roughly 10%.

At present, in view of the sizable experimental error and the theoretic uncertainties, the strong suppression of  $Br(B \rightarrow X_s \gamma)$  by the KK modes does not yet provide a powerful lower bound on  $1/R$  and the values  $1/R \geq 250 \text{ GeV}$  are fully consistent with the experimental result. Once the NNLO calculation is completed and the experimental uncertainties reduced,  $Br(B \rightarrow X_s \gamma)$  may provide a very powerful bound on  $1/R$  that is substantially stronger than the bounds obtained from the electroweak precision data.

The suppression of  $Br(B \rightarrow X_s \gamma)$  in the ACD model has already been found in [4]. Our result presented above is consistent with the one obtained by these authors but differs in details as only the dominant diagrams have been taken into account in the latter paper and the analysis was performed in the LO approximation.

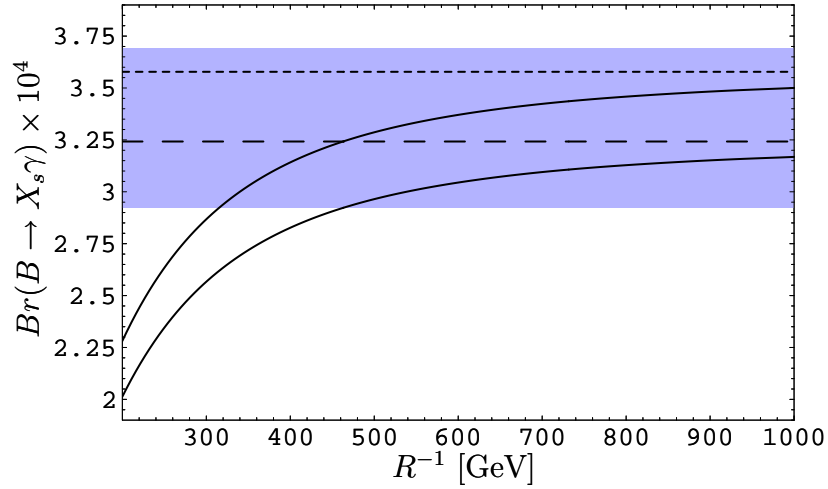


Figure 3.6: The branching ratio for  $B \rightarrow X_s \gamma$  and  $E_\gamma > 1.6$  GeV as a function of  $1/R$ . The meaning of the various curves is explained in the text.

$1/R[\text{GeV}]$	$\mu_b = 2.5 \text{ GeV}$		$\mu_b = 5.0 \text{ GeV}$		$\mu_b = 7.5 \text{ GeV}$	
	Br(LO)	Br(NLO)	Br(LO)	Br(NLO)	Br(LO)	Br(NLO)
200	1.54	2.32	1.02	2.30	0.79	2.28
250	1.92	2.66	1.37	2.65	1.11	2.63
300	2.18	2.89	1.61	2.88	1.35	2.86
400	2.49	3.15	1.90	3.15	1.63	3.13
SM	2.99	3.57	2.39	3.58	2.11	3.56

Table 3.4: The branching ratio for  $B \rightarrow X_s \gamma$  in LO and NLO in units of  $10^{-4}$  as a function of  $1/R$  for  $m_c/m_b = 0.22$  and various values of  $\mu_b$ .

### 3.2.3 Branching Ratio for $B \rightarrow X_s$ gluon

For the decay  $b \rightarrow sg$ , the domination operator is  $Q_{8G}$  and consequently the value of the coefficient  $C_{8G}$  is crucial here. The SM branching ratio is strongly enhanced by NLO QCD corrections [54] with the result

$$Br(b \rightarrow sg) = (5.0 \pm 1.0) \cdot 10^{-3}, \quad m_c/m_b = 0.29. \quad (3.51)$$

Compared to the LO prediction, it is enhanced by a factor of 2.5. Taking  $m_c/m_b = 0.22$ , we find, using the computer program of [54],

$$Br(b \rightarrow sg) = (4.1 \pm 0.7) \cdot 10^{-3}, \quad m_c/m_b = 0.22. \quad (3.52)$$

The uncertainty in  $m_c/m_b$  and the renormalization scale dependence constitute the main uncertainties in the prediction.

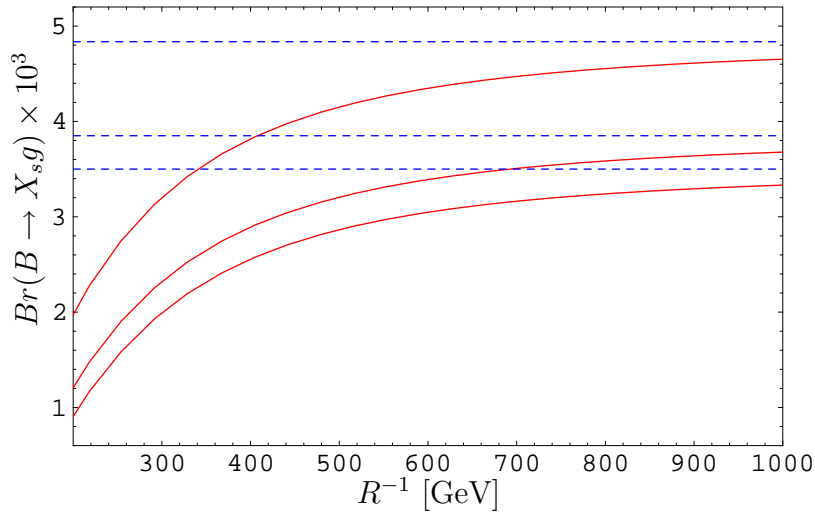


Figure 3.7: The branching ratio for  $B \rightarrow X_s g$  for  $m_c/m_b = 0.22$  and  $\mu_b = 2.5, 5, 7.5$  GeV.  $Br(B \rightarrow X_s g)$  decreases with increasing  $\mu_b$ . The dashed lines represent the SM prediction.

The results for the branching ratio in the ACD model are shown in Fig. 3.7. The dashed lines represent the SM prediction and the solid lines the ACD prediction. The uncertainty is solely due to the renormalization scale dependence. We notice a strong suppression of the branching ratio by the KK modes which is already visible in the LO results of  $C_{8G}^{(0)\text{eff}}(\mu_b)$  in Section 3.2.1.

At present, these results cannot be used to put a lower bound on the compactification scale  $1/R$  in the ACD model. Not only is it still necessary to reduce the large theoretical uncertainties in  $\mu_b$  and  $m_c/m_b$ , also the extraction of the branching ratio from the data turns out to be very difficult, if not impossible. If these obstacles can be overcome, the decay  $B \rightarrow X_s$  gluon could offer a very powerful constraint on  $1/R$ .



### 3.3 The decay $B \rightarrow X_s \mu^+ \mu^-$

The inclusive  $B \rightarrow X_s \mu^+ \mu^-$  decay has been the subject of very intensive theoretical and experimental research during the last 15 years. Like the decay  $B \rightarrow X_s \gamma$ , it is an important testing ground for the flavour structure of the SM and offers a window for exploring new physics at the TeV scale.

#### 3.3.1 Effective Hamiltonian and Branching Ratio

The relevant part of the effective Hamiltonian at scales  $\mu = O(m_b)$  is given by

$$\mathcal{H}_{\text{eff}}(b \rightarrow s \mu^+ \mu^-) = \mathcal{H}_{\text{eff}}(b \rightarrow s \gamma) - \frac{G_F}{\sqrt{2}} V_{ts}^* V_{tb} [C_{9V}(\mu) Q_{9V} + C_{10A}(M_W) Q_{10A}], \quad (3.53)$$

where  $\mathcal{H}_{\text{eff}}(b \rightarrow s \gamma)$  is given in (3.41). There are two new operators  $Q_{9V}$  and  $Q_{10A}$  in addition to those relevant for the decay  $B \rightarrow X_s \gamma$ :

$$Q_{9V} = (\bar{s} \gamma_b)_{V-A} (\bar{\mu} \mu)_V, \quad Q_{10A} = (\bar{s} b)_{V-A} (\bar{\mu} \mu)_A, \quad (3.54)$$

For this decay, a proper treatment of the  $\bar{c}c$  resonances is mandatory. As the theoretical side relies on the domination of perturbative contributions, one has to remove these resonances by appropriate kinematical cuts in the dilepton mass spectrum. Introducing

$$\hat{s} = \frac{(p_{\mu^+} + p_{\mu^-})^2}{m_b^2}, \quad z = \frac{m_c}{m_b}, \quad (3.55)$$

the low dilepton mass window is given by region

$$\left( \frac{2m_\mu}{m_b} \right)^2 \leq \hat{s} \leq \left( \frac{M_{J/\psi} - 0.35 \text{ GeV}}{m_b} \right)^2. \quad (3.56)$$

The theoretical calculations are cleanest for  $\hat{s}_0 \leq 0.25$  where the numerically relevant parts of the NNLO corrections for the inclusive decays are known [55, 56, 57] and resonant effects due to  $J/\psi$ ,  $\psi'$ , etc. are expected to be small.

The experimental value by the BABAR collaboration reads [58]

$$Br(B \rightarrow X_s \mu^+ \mu^-) = (5.0 \pm 2.8 \pm 0.6 \pm 1.0) \cdot 10^{-6}, \quad (3.57)$$

which is consistent with the value reported by the BELLE collaboration [59]

$$Br(B \rightarrow X_s \mu^+ \mu^-) = (4.13 \pm 1.05_{-0.69}^{+0.73}) \cdot 10^{-6}. \quad (3.58)$$

However, these values include the contributions from the full dilepton mass spectrum. Future experimental analyses are supposed to give the results corresponding to the low dilepton mass window so that a direct comparison between experiment and theory will

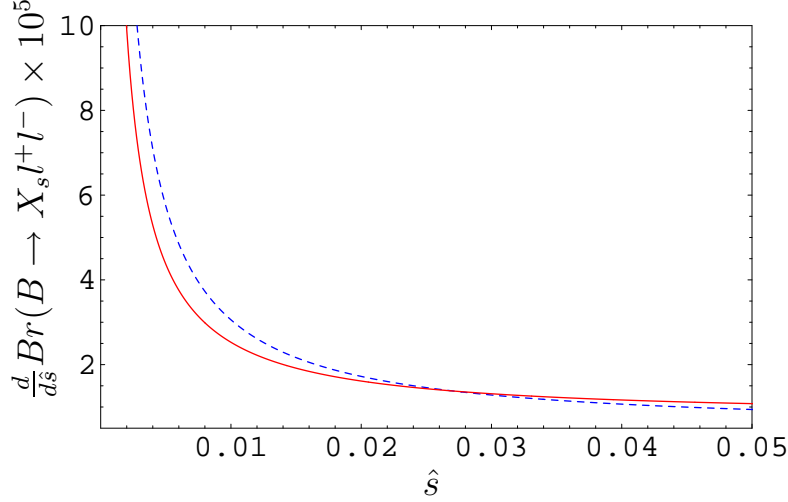


Figure 3.8:  $\frac{d}{d\hat{s}}Br(B \rightarrow X_s l^+ l^-)$  in the SM (dashed line) and the ACD model for  $R^{-1} = 250$  GeV in the low  $\hat{s}$  region.

be possible. At the moment, it is necessary to integrate the theoretical expressions over the whole dilepton mass spectrum [61].

In these two cases, the SM expectations are given by

$$\tilde{Br}(B \rightarrow X_s \mu^+ \mu^-)_{\text{SM}} = (2.75 \pm 0.45) \cdot 10^{-6}, \quad (3.59)$$

where the dilepton mass spectrum has been integrated in the limits suggested by BELLE [60] and given in (3.56), and

$$Br(B \rightarrow X_s \mu^+ \mu^-)_{\text{SM}} = (4.15 \pm 0.7) \cdot 10^{-6}, \quad (3.60)$$

which corresponds to the full dilepton mass spectrum. The predictions of the ACD model ( $1/R = 250$  GeV) for the differential branching ratio in both cases are shown in Fig. 3.8 and Fig. 3.9.

In Fig. 3.10 we show the branching ratio  $\tilde{Br}(B \rightarrow X_s \mu^+ \mu^-)$  as a function of  $1/R$ . In obtaining these results we followed closely the procedure of the authors of [55, 61] and generalized their computer programs to include the KK contributions. We observe a modest enhancement of  $\tilde{Br}(B \rightarrow X_s \mu^+ \mu^-)_{\text{ACD}}$ , corresponding to the low dilepton mass window, that for  $1/R = 300$  GeV amounts to roughly 12%.

For the whole spectrum, we find  $Br(B \rightarrow X_s \mu^+ \mu^-)_{\text{ACD}} = (4.8 \pm 0.8) \cdot 10^{-6}$ . The SM prediction nearly coincides with BELLE's result in (3.58), while the ACD model prediction is closer to BABAR's value in (3.57). However, the large experimental errors and still sizable theoretical uncertainties in the branching ratio corresponding to the full dilepton mass spectrum, also of non-perturbative origin, preclude definite conclusions at present. As we stated before it is safer to consider the branching ratio for the low dilepton mass window as given in in Fig. 3.10.

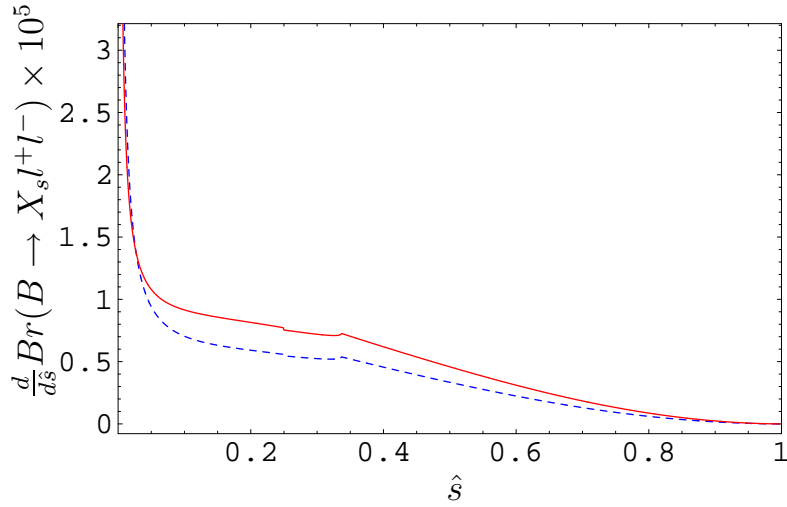


Figure 3.9:  $\frac{d}{d\hat{s}} Br(B \rightarrow X_s l^+ l^-)$  in the SM (dashed line) and the ACD model for  $R^{-1} = 250$  GeV for the full dilepton mass spectrum.

### 3.3.2 Forward-Backward Asymmetry

In the decay  $B \rightarrow X_s \mu^+ \mu^-$ , the forward-backward asymmetry is particularly interesting. At the NLO level where it first becomes non-zero, it is given by [62]

$$A_{\text{FB}}(\hat{s}) = \frac{1}{\Gamma(b \rightarrow ce\bar{\nu})} \int_{-1}^1 d \cos \theta_l \frac{d^2 \Gamma(b \rightarrow s \mu^+ \mu^-)}{d\hat{s} d \cos \theta_l} \text{sgn}(\cos \theta_l) \quad (3.61)$$

$$= -3\tilde{C}_{10} \frac{[\hat{s} \text{Re} \tilde{C}_9^{\text{eff}}(\hat{s}) + 2C_{7\gamma}^{(0)\text{eff}}]}{U(\hat{s})}, \quad (3.62)$$

where  $\theta_l$  is the angle between the  $\mu^+$  and  $B$  meson momenta in the center of mass frame. The function  $U(\hat{s})$  is given by

$$U(\hat{s}) = (1 + 2\hat{s}) \left( |\tilde{C}_9^{\text{eff}}(\hat{s})|^2 + |\tilde{C}_{10}|^2 \right) + 4 \left( 1 + \frac{2}{\hat{s}} \right) |C_{7\gamma}^{(0)\text{eff}}|^2 + 12C_{7\gamma}^{(0)\text{eff}} \text{Re} \tilde{C}_9^{\text{eff}}(\hat{s}), \quad (3.63)$$

and  $\tilde{C}_9^{\text{eff}}(\hat{s})$  is a function of  $\hat{s}$  that depends on the Wilson coefficient  $\tilde{C}_9^{\text{NDR}}$  and includes also contributions from four quark operators [63, 64].

The asymmetry  $A_{\text{FB}}(\hat{s})$  vanishes in exclusive [65] and inclusive decays. In the latter case, the zero of the forward-backward asymmetry is given by

$$\hat{s}_0 \text{Re} \tilde{C}_9^{\text{eff}}(\hat{s}_0) + 2C_{7\gamma}^{(0)\text{eff}} = 0. \quad (3.64)$$

The asymmetry  $A_{\text{FB}}(\hat{s})$  and hence also the value of  $\hat{s}_0$  are sensitive to short-distance physics. As the non-perturbative uncertainties are very small, they provide a particularly useful test for physics beyond the SM.

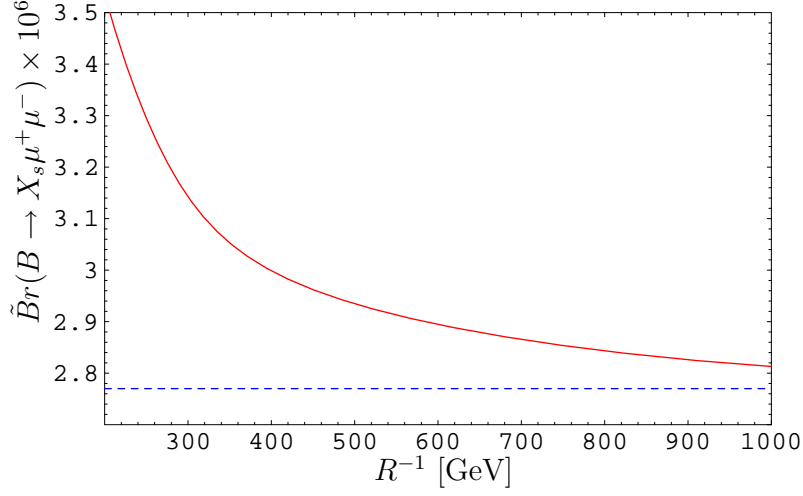


Figure 3.10:  $\tilde{B}r(B \rightarrow X_s \mu^+ \mu^-)$  in the SM (dashed line) and in the ACD model. The integration limits have been chosen as defined in (3.56).

For our analysis, we used the computer program of [55, 61] that includes the sizable NNLO corrections [55, 56], which we modified to include also the KK contributions. In Fig. 3.11 we show the normalized forward-backward asymmetry

$$\hat{A}_{FB}(\hat{s}) = \Gamma(b \rightarrow ce\bar{\nu}) \times A_{FB}(\hat{s}) / \int_{-1}^1 d \cos \theta_l \frac{d^2 \Gamma(b \rightarrow s \mu^+ \mu^-)}{d\hat{s} d \cos \theta_l}. \quad (3.65)$$

In Fig. 3.12 the dependence of  $\hat{s}_0$  on  $1/R$  is shown.

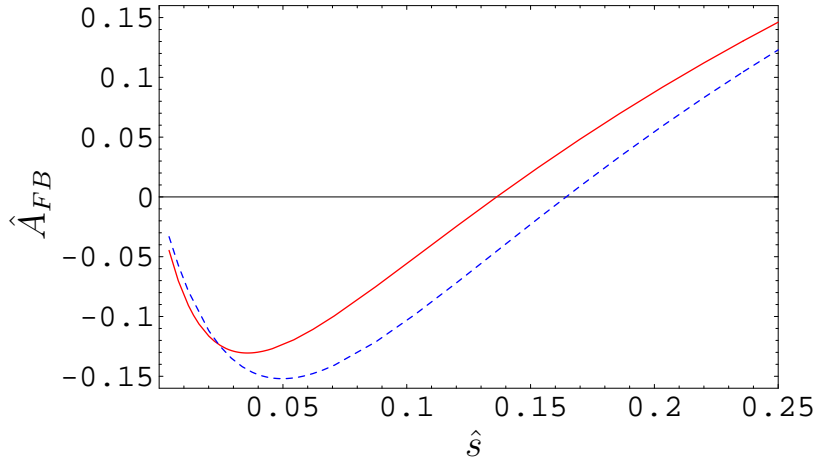


Figure 3.11: Normalized forward-backward asymmetry in the SM (dashed line) and ACD for  $R^{-1} = 250$  GeV.

The coefficient  $\tilde{C}_9^{\text{eff}}$  is only weakly affected by the KK contributions, whereas  $C_{7\gamma}^{(0)\text{eff}}$  is substantially suppressed. Consequently, the value of  $\hat{s}_0$  is considerably reduced relative

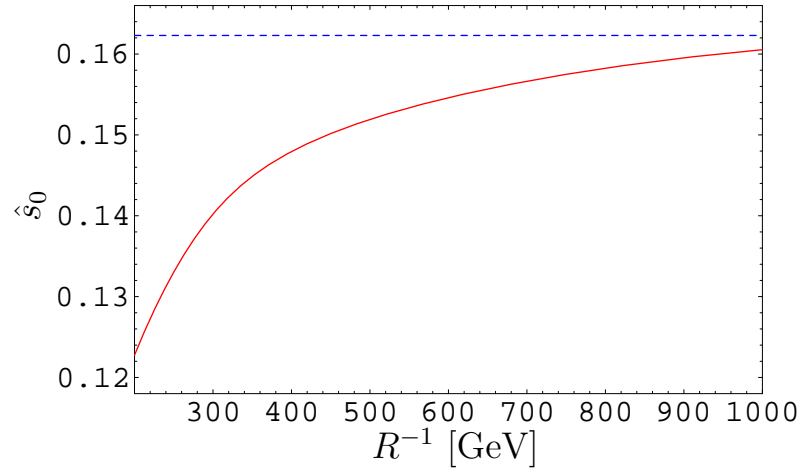


Figure 3.12: Zero of the forward-backward asymmetry  $A_{FB}$  in the SM (dashed line) and the ACD model.

to the SM as can be seen in Fig. 3.12. For  $1/R = 300$  GeV we find a value for  $\hat{s}_0$  that is very close to the NLO prediction of the SM. This demonstrates clearly the importance of the higher order QCD corrections, in particular in quantities like  $\hat{s}_0$  that are theoretically clean. We expect that the results in Fig. 3.11 and Fig. 3.12 will play an important role in the tests of the ACD model in the future.



## Chapter 4

# Dimensional Deconstruction

## 4.1 Framework

The ACD model with one universal extra dimension is not renormalizable. This is generally the case for quantum field theories in more than the usual 4 space-time dimensions. They can be regarded as effective theories valid up to some cut-off scale  $\Lambda$ . A naive cut-off by truncation of the tower of KK modes violates local gauge invariance in the extra dimensions and is therefore inconvenient. A solution to this problem is provided by dimensional deconstruction.

Dimensional deconstruction is the modelling of extra dimensions on a finite lattice of space-time points. It gives rise to two possible interpretations. On the one hand, it can be viewed as a gauge invariant regulator of a higher dimensional theory<sup>1</sup>. The parameters of the deconstructed model are matched to the continuum theory in the low energy limit. In this way, possible influences from physics at the cut-off scale can be studied, although one has to bear in mind that these results are specific to this particular UV completion and may not be generally true in others.

On the other hand, dimensional deconstruction stands on its own right as a framework for model building, and a correspondence to continuous extra dimensions is not necessary. There is a great freedom in choosing the topology, particle content and couplings, to which the analogy to extra dimensions may be used as a guiding principle. Although the model we consider in this work is an emulation of a continuous extra dimension, we always interpret our results regarding both points of view.

The simplest geometry for a compact extra dimension is the circle  $S^1$ . In dimensional deconstruction the corresponding moose diagram is a circle consisting of discrete lattice points, where the matter and gauge fields live, connected by linking Higgs fields.

In higher dimensional models, chiral fermions are realized by orbifold compactifications. The simplest possibility is the orbifold  $S^1/Z_2$  which is in dimensional deconstruction implemented by an aliphatic setup [12]. The moose diagram consists of a line with its two endpoints corresponding to the fixed points of the orbifold. This aliphatic structure can have the matter fields living on every lattice site [12] corresponding to the UED models [2] where all fields live in the bulk. It is also possible to have only the gauge fields in the bulk and place the fermions on specific sites [66].

In this thesis we study an aliphatic model with chiral fermions on the lattice sites together with a replicated  $U(1)$  as the gauge group. This is the deconstructed version of a 5D UED theory with a chiral fermion, compactified on the orbifold  $S^1/Z_2$ . In this section we discuss the Lagrangian of the model.

### 4.1.1 Gauge field lattice

First we consider the deconstruction of a 5D  $U(1)$  gauge theory. We have  $N + 1$  lattice sites connected by  $N$  linking Higgs fields in the bifundamental representation of their neighbouring gauge groups, see Fig. 4.1. The Lagrangian for this moose diagram reads

---

<sup>1</sup>Other regularization schemes of higher dimensional field theories have been discussed in [13].



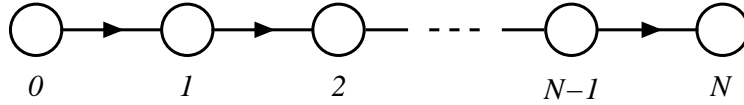


Figure 4.1: Moose diagram of the aliphatic model. The circles denote the lattice sites with the gauge fields, connected by the linking Higgs fields.

$$\mathcal{L} = -\frac{1}{4} \sum_{n=0}^N F_{\mu\nu n} F_n^{\mu\nu} + \sum_{n=1}^N (D_\mu \Phi_n)^\dagger (D^\mu \Phi_n) - V(\Phi) \quad (4.1)$$

with the covariant derivative

$$D_\mu \Phi_n = [\partial_\mu - igA_{\mu n-1} + igA_{\mu n}] \Phi_n. \quad (4.2)$$

The link field  $\Phi_n$  connects the lattice sites  $n-1$  and  $n$ .

In higher dimensional models, the masses of the KK excitations are generated by derivative terms along the extra dimensions. This leads to a linear spectrum of a tower of KK modes which is universal for all fields. In dimensional deconstruction the KK masses are basically generated by the vacuum expectation value (VEV) of the linking Higgs field. The Higgs potential  $V(\Phi)$  is chosen such that every  $\Phi_n$  gets a universal VEV

$$\langle \Phi_n \rangle = \frac{v}{\sqrt{2}g}, \quad (4.3)$$

where we have included a factor of  $1/\sqrt{2}g$  for notational simplicity. This VEV spontaneously breaks local gauge invariance in the latticized fifth dimension and gives masses to the gauge boson KK modes. The associated Goldstone bosons are the imaginary parts of the complex fields  $\Phi_n$ .

The mass term of the gauge fields

$$\frac{1}{2} v^2 \sum_{n=1}^N (A_{\mu n-1} - A_{\mu n})^2 \quad (4.4)$$

originates from the linking Higgs kinetic terms, where  $\Phi_n$  is replaced by its VEV. It is diagonalized by

$$A_{n,\mu} = \sqrt{\frac{2}{N+1}} \sum_{k=0}^N \left( \frac{1}{\sqrt{2}} \right)^{\delta_k} \cos \frac{(n+1/2)k\pi}{N+1} A_{\mu(k)}, \quad (4.5)$$

giving the masses

$$m_{A(k)} = 2v \sin \frac{k\pi}{2(N+1)}. \quad (4.6)$$

We have put parentheses around the KK mode number to distinguish the KK mass eigenstates from the position eigenstates in lattice space.

In the low-energy limit  $k \ll N$  we can identify the parameters of the orbifold model with those in the deconstructed setup. The mass spectrum is then approximately linear:

$$m_{A^{(k)}} \approx \frac{vk\pi}{N+1} \leftrightarrow \frac{k}{R}, \quad (4.7)$$

where  $R$  is the radius of the orbifold. Introducing the lattice spacing  $a$  we can identify  $\pi R = (N+1)a$  and get the tree-level relation  $v = 1/a$ . One could say that for fixed  $N$  the size of the deconstructed dimension is given dynamically by the VEV of the link field.<sup>2</sup>

For the fields  $\Phi_n$  we work with the linear representation

$$\Phi_n = \frac{v}{\sqrt{2}g} + \frac{1}{\sqrt{2}}(\Sigma_n + iG_n), \quad (4.8)$$

where the  $G_n$  are the Goldstone modes and the  $\Sigma_n$  are physical real scalars. We apply an  $R_\xi$ -gauge fixing similar to the one used in the periodic case for the non-linear realization of the gauge symmetry [22]:

$$\mathcal{L}_{\text{GF}} = -\frac{1}{2} \sum_{n=0}^N \mathcal{G}_n^2 \quad (4.9)$$

with

$$\mathcal{G}_n = \frac{1}{\sqrt{\xi}} [\partial_\mu A_n^\mu + v\xi(G_{n+1} - G_n)] \quad (4.10)$$

and  $G_{N+1} \equiv 0$ . The gauge fixing generates mass terms for the Goldstone modes which are diagonalized by

$$G_n = \sqrt{\frac{2}{N+1}} \sum_{k=1}^N \sin \frac{nk\pi}{N+1} G^{(k)}, \quad (4.11)$$

resulting in the masses

$$m_{G^{(k)}} = \sqrt{\xi} 2v \sin \frac{k\pi}{2(N+1)}. \quad (4.12)$$

Not surprisingly, the masses of the Goldstone bosons are the same as in (4.6) with an additional factor of  $\sqrt{\xi}$ .

The Higgs potential can in principle contain any renormalizable, gauge invariant combination of the  $\Phi_n$ . The simplest choice is

$$V(\Phi) = \sum_{n=1}^N \left[ -\mu^2 \Phi_n^\dagger \Phi_n + \frac{\lambda}{2} (\Phi_n^\dagger \Phi_n)^2 \right]. \quad (4.13)$$

---

<sup>2</sup>See [67] for a discussion of nonperturbative corrections to the radius.

Here the  $\Phi_n$  are decoupled from each other in the potential, and after spontaneous symmetry breaking (SSB) the VEV is given by (4.3). The physical modes  $\Sigma_n$  get the universal mass  $m_\Sigma = \sqrt{2}\mu = \sqrt{\lambda}v/g$ , with its natural value given by the cutoff of the 4-dimensional theory. The  $\Sigma_n$  are degenerate in mass, so we are free to carry out an arbitrary orthogonal transformation on them. For the purpose of analogy to the Goldstone modes, we transform the mass eigenstates  $\Sigma_n$  to  $\Sigma_{(n)}$  as in (4.11).

By taking the limit  $\mu \rightarrow \infty, \lambda \rightarrow \infty$  while keeping the Higgs VEV fixed, we can make the  $\Sigma_n$  arbitrary heavy, decoupling them from low-energy dynamics. It can then be useful to switch to a non-linear sigma model representation

$$\Phi_n \longrightarrow \frac{v}{\sqrt{2}g} \exp(ig\phi_n/v) \quad (4.14)$$

that reflects the role of the linking Higgs as a Wilson line [12]. The physical modes are eliminated at the price of leaving a non-renormalizable theory. At low energies this non-linear sigma model is indistinguishable from the linear sigma model. The choice of one representation is just a matter of convenience [11]. As we are mainly interested in the renormalizability of the model, we will use the linear representation given by (4.8).

A remark is in order here about more complicated Higgs potentials. Even if we restrict ourselves to renormalizable operators, we can introduce couplings between different lattice sites, for example the nearest neighbour coupling

$$V'(\Phi) = V(\Phi) + \lambda' \sum_{n=0}^{N-1} \Phi_n^\dagger \Phi_n \Phi_{n+1}^\dagger \Phi_{n+1}. \quad (4.15)$$

The tree level minimum of the potential is then no longer given by a universal VEV, although KK parity is still respected, that is  $\langle \Phi_n \rangle = \langle \Phi_{N+1-n} \rangle$ . This results in a change of the mode expansion, masses and couplings of the fields. If we let us guide by locality in 5D, it is natural to assume that couplings between distant lattice sites are suppressed ( $\lambda' \ll \lambda$ ). However, from the point of view of moose model building there is no fundamental reason which dictates locality<sup>3</sup>.

In the general case there can appear terms coupling arbitrary lattice sites with each other. Moreover, the individual couplings do not necessarily have to be universal but can depend on the individual lattice sites. The freedom of non-universal VEVs and couplings can be used to build models that describe warped backgrounds [18, 19]. In the remainder of this work, we will use (4.13), which ensures, at least at tree level, a universal VEV for all  $\Phi_n$ .

### 4.1.2 Fermions in the aliphatic setup

We consider the deconstructed version of a higher dimensional model similar to the one studied in [69, 26]. Relevant for us is the occurrence of a fermion in 5D with a chiral zero-mode. As has been pointed out in [70], the analogy of the deconstructional setup to the

---

<sup>3</sup>Examples of strictly non-local theory spaces can be found in [68].

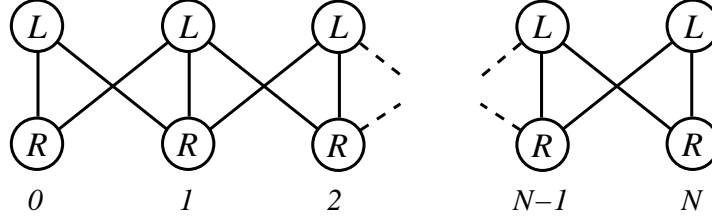


Figure 4.2: The lattice of the fermions without the Wilson term. The vertical lines represent the bare mass terms. The diagonal lines represent the link fields which connect fermions of neighbouring lattice sites.

continuous case is not obvious, since the orbifold boundary conditions cannot be directly translated to the lattice. In this section we review the construction of the Lagrangian of the fermions, following the presentation of [71], where the periodic lattice was considered.

We start with  $2N + 2$  chiral fermions that are charged under the  $U(1)$  of their lattice site. The kinetic term reads

$$\sum_{n=0}^N [\bar{\psi}_{Ln} i \not{D} \psi_{Ln} + \bar{\psi}_{Rn} i \not{D} \psi_{Rn}], \quad (4.16)$$

with the covariant derivative

$$D_\mu \psi_{L/Rn} = (\partial_\mu + ig A_{\mu n}) \psi_{L/Rn}. \quad (4.17)$$

We couple the linking Higgs to the fermions in such a way that the imaginary (unphysical) part of the scalar can be identified with the fifth component of the  $U(1)$  vector field coupled covariantly to the fermions. We also introduce a bare mass term coupling two chiral fermions of the same lattice site:

$$\sum_{n=0}^N \left[ -M \bar{\psi}_n \psi_n - \frac{1}{\sqrt{2}} g \eta (\bar{\psi}_{n-1} \gamma_5 \Phi_n \psi_n + \text{h.c.}) \right], \quad (4.18)$$

with  $\psi_n \equiv \psi_{Ln} + \psi_{Rn}$ . This setup is illustrated in Fig. 4.2. In order to remedy the fermion doubling problem, we have to introduce a Wilson term

$$\sum_{n=0}^N \left\{ v \eta' \bar{\psi}_n \psi_n - \frac{1}{\sqrt{2}} g \eta' (\bar{\psi}_{n-1} \Phi_n \psi_n + \text{h.c.}) \right\}. \quad (4.19)$$

The coupling between the fermions and the Higgs field is given by a dimensionless constant  $\eta'$ , and the parameter  $v$  is set to match the Higgs VEV. Putting (4.18) and (4.19) together we get

$$\sum_{n=0}^N \left\{ -(M - v \eta') \bar{\psi}_n \psi_n - \frac{1}{\sqrt{2}} g \left( [\bar{\psi}_{Ln-1} \Phi_n \psi_{Rn} + \bar{\psi}_{Rn} \Phi_n^\dagger \psi_{Ln-1}] (\eta' + \eta) \right. \right. \\ \left. \left. + [\bar{\psi}_{Rn-1} \Phi_n \psi_{Ln} + \bar{\psi}_{Ln} \Phi_n^\dagger \psi_{Rn-1}] (\eta' - \eta) \right) \right\}. \quad (4.20)$$

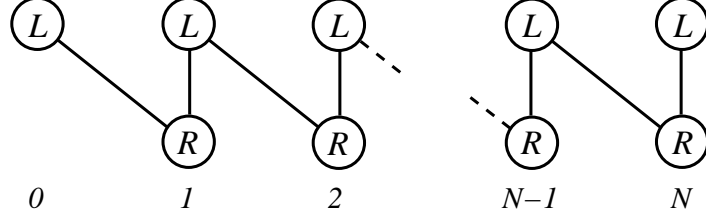


Figure 4.3: The lattice of the fermions after elimination of half of the links by the Wilson term and removal of one of the right-handed modes.

In order to eliminate half of the links between two adjacent sites, we set  $\eta' = \eta$ . This leaves us with

$$\sum_{n=0}^N \left\{ -\tilde{M} \bar{\psi}_n \psi_n - \sqrt{2} g \eta \left[ \bar{\psi}_{L_{n-1}} \Phi_n \psi_{Rn} + \bar{\psi}_{Rn} \Phi_n^\dagger \psi_{L_{n-1}} \right] \right\}, \quad (4.21)$$

where  $\tilde{M} = M - v\eta$ . Inserting the Higgs VEV (4.3) we get the mass terms

$$\sum_{n=0}^N \left\{ -\tilde{M} \left[ \bar{\psi}_{L_n} \psi_{Rn} + \bar{\psi}_{Rn} \psi_{L_n} \right] - v\eta \left[ \bar{\psi}_{L_{n-1}} \psi_{Rn} + \bar{\psi}_{Rn} \psi_{L_{n-1}} \right] \right\}. \quad (4.22)$$

The “kink”-mass  $M$  in the Lagrangian yields an offset of  $M^2$  in the fermion mass spectrum [70, 71]. In order to end up with an orbifold-like mass spectrum, we have to set  $M = 0$  and therefore  $\tilde{M} = -v\eta$ . The mass terms then read

$$-v\eta \sum_{n=0}^N \left[ (\bar{\psi}_{L_{n-1}} - \bar{\psi}_{L_n}) \psi_{Rn} + \text{h.c.} \right]. \quad (4.23)$$

This last step is actually a fine-tuning of the parameters, since the parameter  $v$  in (4.23) has two different origins. The term coupling two fermions of neighbouring lattice sites is generated by SSB, where the linking Higgs field is replaced by its VEV. On the other hand, in the coupling of two fermions of the same site we have put in the VEV by hand in (4.19) and by setting  $M = 0$ . We can do so at tree level, but as we will see later, radiative corrections spoil this naive choice.

We want a single chiral zero-mode, which is accomplished by setting  $\psi_{R0} \equiv 0$ . The sums in (4.21) and (4.23) now run from 1 to  $N$ :

$$\sum_{n=1}^N \left\{ v\eta \bar{\psi}_n \psi_n - \sqrt{2} g \eta \left[ \bar{\psi}_{L_{n-1}} \Phi_n \psi_{Rn} + \bar{\psi}_{Rn} \Phi_n^\dagger \psi_{L_{n-1}} \right] \right\}. \quad (4.24)$$

This is illustrated in Fig. 4.3. For the fermion masses, we get the terms

$$-v\eta \sum_{n=1}^N \left[ (\bar{\psi}_{L_{n-1}} - \bar{\psi}_{L_n}) \psi_{Rn} + \text{h.c.} \right] = -(\bar{\psi}_{L_0}, \dots, \bar{\psi}_{L_N}) \hat{M} (\psi_{R1}, \dots, \psi_{RN})^T + \text{h.c.} \quad (4.25)$$

The  $(N + 1) \times N$  mass matrix  $\hat{M}$  takes the form

$$\hat{M} = v\eta \begin{pmatrix} 1 & 0 & 0 & \dots & 0 \\ -1 & 1 & 0 & \dots & 0 \\ 0 & -1 & 1 & \dots & 0 \\ \dots & \dots & \dots & \dots & \dots \\ 0 & \dots & \dots & -1 & 1 \\ 0 & \dots & \dots & 0 & -1 \end{pmatrix}. \quad (4.26)$$

It is diagonalized by

$$\psi_{Ln} = \sqrt{\frac{2}{N+1}} \sum_{k=0}^N \left(\frac{1}{\sqrt{2}}\right)^{\delta_k} \cos \frac{(n+1/2)k\pi}{N+1} \psi_{L(k)}, \quad (4.27)$$

$$\psi_{Rn} = \sqrt{\frac{2}{N+1}} \sum_{k=1}^N \sin \frac{nk\pi}{N+1} \psi_{R(k)}, \quad (4.28)$$

resulting in the fermion masses

$$m_{\psi(k)} = 2v\eta \sin \frac{k\pi}{2(N+1)}. \quad (4.29)$$

Getting the same mass spectrum as for the gauge bosons (4.6) requires the choice of  $\eta = 1$ . This also justifies the ad-hoc setting  $M = 0$ . In the following, we keep the parameter  $\eta$  explicitly in all expressions in order to keep track of the various contributions to our results.

For arbitrary  $M$  and  $\eta$  we would get the mass spectrum

$$m_{\psi(k)}^2 = M^2 + 4(v\eta - M)v\eta \sin^2 \frac{k\pi}{2(N+1)}, \quad k \geq 1. \quad (4.30)$$

The zero-mode  $\psi_{(0)}$  must always stay massless, even for  $M \neq 0$ , since it has no chiral partner. In a phenomenologically realistic setup, two sets of fermions, one with a left-handed zero-mode and one with a right-handed zero-mode, would be coupled to a Higgs field. After SSB at the electroweak scale, the usual SM fermion masses for the zero-modes arise. This also remedies the possible occurrence of gauge anomalies that are generally present in a setup with chiral fermions. However, this issue is not important for the calculation of the fermion self-energies in the next section.

## 4.2 Feynman rules and Kaluza-Klein parity

In order to be a gauge invariant, renormalizable UV completion of a higher dimensional theory, the deconstructed theory not only has to possess the same mass spectrum in the low energy limit. It is essential that the Feynman rules are also equivalent and important properties of the higher dimensional theory are reproduced.

In orbifold theories translational Lorentz symmetry is broken at the fixed points, and the momentum in the extra dimensions is no longer conserved. However, if the field content is appropriately chosen, for example in models with universal extra dimensions, there is a discrete remnant of this symmetry that is still intact, namely Kaluza-Klein parity. This is the reflection generated by the transformation  $y \rightarrow \pi R - y$ , where  $y$  is the coordinate in the extra dimension.

The conservation of KK parity is an important property of UED models. It causes the lightest KK particle (LKP) to be stable, providing an excellent candidate for dark matter in orbifold extensions of the SM [72]. Apart from that, it also implies the absence of tree level KK contributions to low energy processes taking place at scales  $\mu \ll 1/R$ . In FCNC processes it is responsible for the GIM mechanism to improve the convergence of the sum over KK modes and for the relatively mild impact of the KK modes [3] as opposed to models with fermions localized on a brane [73]. For these reasons the phenomenological bounds on the compactification scale are typically much weaker [2, 3, 4, 6, 10, 74] than in non-universal extra dimensions. In order for the deconstructed theory to be a faithful low-energy representation of such a 5-dimensional model, it is essential that KK parity is at least approximately conserved, possibly violated only at a high scale.

We will see that the one-loop corrections to the fermion masses exhibit a structure quite different from orbifold theories. We therefore take a closer look at the Feynman rules of the aliphatic model in terms of mass eigenstates in this section. We especially elaborate to which extent KK parity is reflected in the Lagrangian. We take the coupling of the gauge bosons to the fermions and to the link fields as examples to show the analogies and differences to the corresponding orbifold model.

Before we discuss the individual vertices, let us briefly review the impact of KK parity on correlation functions. In general, we define a parity transformation by its action on mass eigenstates in order to obtain a definite selection rule. There are two cases relevant for us:

$$i) \phi'_{(k)} = \mp \phi_{(k)} \quad \text{or} \quad ii) \phi'_{(k)} = \pm \phi_{(k)}, \quad (4.31)$$

where  $\phi$  stands for any field in the Lagrangian and the upper (lower) sign is relevant for  $k$  odd (even). We assign to every field either  $i)$  or  $ii)$  such that the Lagrangian is invariant under the transformation.

Let us take the two-point function as an example to show how selection rules for correlation functions can be derived. The generalization to higher correlation functions is obvious. If we assume that all fields transform as  $i)$ , we get

$$\langle \phi'_{(k)} \phi'_{(k')} \rangle = \mp \langle \phi_{(k)} \phi_{(k')} \rangle, \quad (4.32)$$

where we have a minus (plus) sign if  $k - k'$  is odd (even). If the Lagrangian is invariant under  $\phi \rightarrow \phi'$  then the correlation functions for the primed fields are the same as for the unprimed ones, and consequently (4.32) must be zero if  $k - k'$  is odd.

Now we can discuss the Feynman rules and the violation of KK parity. First we note that the transformations into mass eigenstates (4.5), (4.11) and (4.27) are orthogonal and yield canonically normalized kinetic terms for all fields.

For the moment we ignore the fermions. In the aliphatic model the link fields couple to the gauge fields by the covariant derivative. The  $\Phi^\dagger A \Phi$  vertex is given by

$$\begin{aligned} -ig \sum_{n=1}^N \partial_\mu \Phi_n^\dagger (A_{n-1}^\mu - A_n^\mu) \Phi_n + \text{h.c.} &= \frac{-ig}{2} \left( \frac{2}{N+1} \right)^{3/2} \sum_{k,l,m} \partial_\mu \Phi_{(k)}^\dagger A_{(l)}^\mu \Phi_{(m)} \\ &\times \left( \frac{1}{2} \right)^{\delta_l} \sin \frac{l\pi}{2(N+1)} \sum_{n=1}^N \sin \frac{nk\pi}{N+1} \sin \frac{nl\pi}{N+1} \sin \frac{nm\pi}{N+1} + \text{h.c.} . \end{aligned} \quad (4.33)$$

The sum over  $n$  in the second line is given by

$$\frac{1}{4} [\Xi(k+l-m) - \Xi(k-l-m) + \Xi(k-l+m) - \Xi(k+l+m)] \quad (4.34)$$

with (see e.g. [75])

$$\Xi(j) \equiv \sum_{n=1}^N \sin \frac{nj\pi}{N+1} = \sin \frac{Nj\pi}{2(N+1)} \sin \frac{j\pi}{2} \sin^{-1} \frac{j\pi}{2(N+1)}. \quad (4.35)$$

Since  $\Xi(j)$  vanishes for any even  $j$ , we find that KK parity is violated maximally at each vertex of a Feynman diagram.

This can be directly seen in terms of position eigenstates on the lattice. The charge assignment of the  $\Phi_n$  induces a direction on the lattice, hence the  $A_{\mu n}$  must change sign under reflection for (4.33) to be invariant:

$$\Phi_n \longrightarrow \Phi_{N+1-n}, \quad A_{\mu n} \longrightarrow -A_{\mu N-n}. \quad (4.36)$$

The mass eigenstates transform accordingly as *ii*)

$$\begin{aligned} \Phi'_{(k)} &= \sum_{n=1}^N \sin \frac{nk\pi}{N+1} \Phi_{N+1-n} = \pm \Phi_{(k)}, \\ A'_{\mu(k)} &= \sum_{n=0}^N \cos \frac{(n+1/2)k\pi}{N+1} (-A_{\mu N-n}) = \pm A_{\mu(k)}. \end{aligned} \quad (4.37)$$

For correlation functions with an even number of fields KK parity is still conserved, while it is violated maximally for an odd number of fields. In the latter case only those correlation functions do not vanish which break KK parity, i.e. if the sum of external KK



numbers  $k_1 + \dots + k_n$  is odd. Although the imaginary parts  $G_n$  of the link fields  $\Phi_n$  can be removed by a gauge transformation, the real parts  $\Sigma_n$  are physical and KK parity is violated at the scale given by their mass.

The four-field vertex  $\Phi^\dagger A A \Phi$  also has no counterpart in the higher dimensional theory. Due to the quadratic occurrence of the gauge fields, KK parity is conserved here.

The situation gets more complicated once we introduce fermions. The coupling of the left-handed fermions to the gauge fields given by the covariant derivative reads

$$\begin{aligned}
& -g \sum_{n=0}^N \bar{\psi}_{nL} \mathcal{A}_{\mu n} \psi_{nL} = -g \left( \frac{2}{N+1} \right)^{3/2} \sum_{k,l,m=0}^N \bar{\psi}_{L(k)} \mathcal{A}_{\mu(l)} \psi_{L(m)} \\
& \times \left( \frac{1}{\sqrt{2}} \right)^{\delta_k + \delta_l + \delta_m} \sum_{n=0}^N \cos \frac{(n+1/2)k\pi}{N+1} \cos \frac{(n+1/2)l\pi}{N+1} \cos \frac{(n+1/2)m\pi}{N+1} \\
& = -\frac{g}{\sqrt{2(N+1)}} \sum_{k,l,m=0}^N \left( \frac{1}{\sqrt{2}} \right)^{\delta_k + \delta_l + \delta_m} \bar{\psi}_{L(k)} \mathcal{A}_{\mu(l)} \psi_{L(m)} \hat{\delta}_{klm}, \tag{4.38}
\end{aligned}$$

where

$$\hat{\delta}_{klm} = \hat{\delta}_{k+l-m} + \hat{\delta}_{k-l-m} + \hat{\delta}_{k-l+m} + \hat{\delta}_{k+l+m} \tag{4.39}$$

and  $\hat{\delta}_k$  is a modified Kronecker delta symbol defined by ( $n \in \mathbb{Z}$ )

$$\hat{\delta}_k = \begin{cases} 1 & \text{if } k = 4n(N+1), \\ -1 & \text{if } k = (4n+2)(N+1), \\ 0 & \text{else.} \end{cases} \tag{4.40}$$

The evaluation of the sum over  $n$  in (4.38) is given in Appendix C.

This result should be compared with the corresponding orbifold model where the  $\hat{\delta}_{k \pm l \pm m}$  in (4.39) are replaced by the ordinary Kronecker  $\delta_{k \pm l \pm m}$  symbols. The difference is due to the fact that the lattice constitutes a discrete dimension and hence multiples of the mode number  $2(N+1)$  are equivalent to the mode number 0.

Despite of this discrepancy, KK parity is conserved here. The term (4.38) is invariant under the transformation

$$\psi_{Ln} \longrightarrow \psi_{LN-n}, \quad A_{\mu n} \longrightarrow A_{\mu N-n}, \tag{4.41}$$

which implies

$$\begin{aligned}
\Psi'_{L(k)} &= \sum_{n=1}^N \cos \frac{(n+1/2)k\pi}{N+1} \psi_{LN-n} = \mp \psi_{L(k)}, \\
A'_{\mu(k)} &= \sum_{n=0}^N \cos \frac{(n+1/2)k\pi}{N+1} A_{\mu N-n} = \mp A_{\mu(k)}. \tag{4.42}
\end{aligned}$$

Note that since the transformation for  $A_\mu$  in (4.41) is different from (4.36), correlation functions involving  $A_\mu$  with both  $\Phi$  and  $\psi_L$  fields do not obey simple selection rules.

For the right-handed fermions we have

$$\begin{aligned}
-g \sum_{n=1}^N \bar{\psi}_{nR} A_{\mu n} \psi_{nR} &= -g \left( \frac{2}{N+1} \right)^{3/2} \sum_{k,l,m=0}^N \bar{\psi}_{R(k)} A_{\mu(l)} \psi_{R(m)} \\
&\times \left( \frac{1}{\sqrt{2}} \right)^{\delta_i} \sum_{n=1}^N \sin \frac{nk\pi}{N+1} \cos \frac{(n+1/2)l\pi}{N+1} \sin \frac{nm\pi}{N+1}.
\end{aligned} \tag{4.43}$$

The sum over  $n$  in the second line is given by

$$\begin{aligned}
&\frac{1}{4} \left[ (N+1) \cos \frac{l\pi}{2(N+1)} \tilde{\delta}_{klm} - \sin \frac{l\pi}{2(N+1)} \right. \\
&\times \left. [\Xi(k+l-m) - \Xi(k-l-m) + \Xi(k-l+m) - \Xi(k+l+m)] \right],
\end{aligned} \tag{4.44}$$

where

$$\tilde{\delta}_{klm} = \check{\delta}_{k+l-m} + \check{\delta}_{k-l-m} - \check{\delta}_{k-l+m} - \check{\delta}_{k+l+m} \tag{4.45}$$

and ( $n \in \mathbb{Z}$ )

$$\check{\delta}_j = \begin{cases} 1 & \text{if } j = 2n(N+1), \\ 0 & \text{else,} \end{cases} \tag{4.46}$$

not to be confused with  $\hat{\delta}_j$  as defined in (4.40). The first term in (4.44) is similar to the corresponding vertex in the orbifold model, while the second term is proportional to the  $\Phi^\dagger A_\mu \Phi$  vertex in (4.33).

This vertex differs substantially from the orbifold vertex because it is not invariant under KK parity transformation

$$\psi_{Rn} \longrightarrow \psi_{RN-n-1}, \quad A_{\mu n} \longrightarrow A_{\mu N-n}. \tag{4.47}$$

It is invariant under the transformation

$$\psi_{Rn} \rightarrow \psi_{RN-n-1}, \quad A_{\mu n} \rightarrow A_{\mu N-n-1}, \tag{4.48}$$

but this does not lead to a definite transformation of the mass eigenstates  $A_{\mu(k)}$ .

The coupling of the linking Higgs field to the fermions is given by (4.24). In terms of mass eigenstates it shows a structure similar to (4.44), only the second term comes with the opposite sign. Again there is no equivalent to this KK parity violating term in the orbifold theory.

We have seen that KK parity is generically violated in the aliphatic setup. As a direct consequence, fields with different KK parity can mix under renormalization. This can be seen explicitly in the structure of the fermion self-energies in Appendix D.

In the case of the linking Higgs field the violation of KK parity can be partially removed by a suitable gauge transformation, while the remaining KK parity violating interactions are suppressed by the mass of the physical scalars. This is no more possible once fermions are introduced in the bulk, and KK parity is violated even at low energies, that is for mode numbers  $k \ll N$ . The lack of symmetry is apparent in Fig. 4.1 and Fig. 4.3, and the cause is twofold.

First, the coupling of fermions to the linking Higgs induces a direction on the lattice quite analogous to the direction induced by the gauge field on the linking Higgs, even in equation (4.18) before the Wilson term is introduced. This is a general feature of deconstruction models where the link field, introduced to give masses to the KK modes by its VEV, is coupled in a gauge invariant way to the other fields.

The second cause is the elimination of  $\psi_{R0}$  that was done to end up with a single massless chiral zero-mode. We have to choose some sort of boundary conditions such that there is a surplus fermion of one chirality. As a fermion without a chiral partner will always stay massless, we end up with one chiral zero-mode. For boundary conditions given at the endpoints of the lattice this means that the two endpoints have to be treated differently if one does not want to eliminate two modes at once.

A remark is in order here about a different class of deconstruction models where fermions live on unique lattice sites [66]. They emulate non-universal extra dimensions where fermions are placed at a brane and KK parity is not conserved. As we have seen above, the most severe troubles in deconstructed UED models come from the fermions in the bulk. Hence all the considerations above involving fermions do not apply here. With only gauge fields and the link fields in the bulk, the Feynman rules will resemble more closely those of an extra dimensional theory. The Goldstone modes can be gauged away and effects of the physical scalars will be suppressed by their mass. For these reasons it seems to us that models with fermions on branes are particularly suited for dimensional deconstruction.

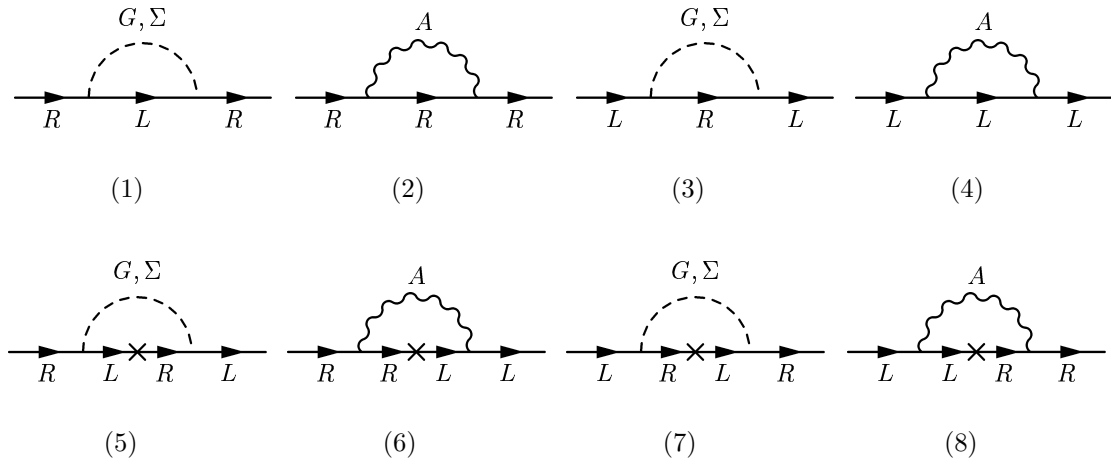


Figure 4.4: One-loop diagrams contributing to the fermion self-energy.

### 4.3 Fermion counter terms and mass shift

In higher dimensional orbifold models, bulk interactions generally induce divergent brane couplings [26]. In two-point functions with different incoming and outgoing 5D momenta (KK mode numbers), there are at the one-loop level only two non-vanishing contributions out of the infinite sum over the KK modes running inside the loop. This is due to the partial conservation of the 5D momentum at each vertex. The divergencies originate from the 4D momentum loop integrals and do not depend on the finiteness of the sum over KK modes.

The models in dimensional deconstruction are designed to emulate their higher-dimensional counterparts in the low energy limit, but differ for high energies. It is therefore not expected that the divergent parts of Feynman amplitudes coincide. However, the divergencies are connected with the renormalization group running of the parameters in the Lagrangian. In [21] the running contribution from the cut-off scale down to the mass scale of the respective KK excitations was extracted from the divergent parts of the self-energies, assuming that the boundary terms vanish at the cut-off scale. Under the assumption of this renormalization condition, these divergencies give rise to a shift in the KK mass spectrum that would be observable at the LHC.

In the following we present the divergent part of the fermion self-energy diagrams and identify the structure of the counterterms needed for renormalization. The relevant 1-loop diagrams are depicted in Fig. 4.4. The scalar tadpole diagrams are finite after renormalization and do not contribute. The diagrams (1)-(4) describe transitions between fermions of the same chirality. The diagrams (5)-(8) are chirality changing and do not contribute to the amplitude proportional to  $\not{p}$  and to the field strength renormalization.

The explicit calculation of the fermion self-energy is illustrated in Appendix D. The

divergent part of the induced counterterms are given by

$$\begin{aligned} \mathcal{L}_{\text{c.t.}} = & \frac{1}{\epsilon} \frac{g^2}{16\pi^2} \left\{ (\eta^2 + 1) \sum_{n=1}^N \bar{\psi}_{Rn} \not{p} \psi_{Rn} + (\eta^2 + 1) \sum_{n=0}^N \bar{\psi}_{Ln} \not{p} \psi_{Ln} - \eta^2 \bar{\psi}_{LN} \not{p} \psi_{LN} \right. \\ & \left. + 4v\eta \sum_{n=1}^N \bar{\psi}_n \psi_n \right\}. \end{aligned} \quad (4.49)$$

We see that there is a boundary contribution to the field strength renormalization of  $\psi_{LN}$  which does not respect the ‘‘hopping’’ symmetry of the Lagrangian. This is not entirely surprising, since this symmetry is broken in the Lagrangian at the end points. It is in fact remarkable that the only effect at the one-loop level is in the  $\not{p}$  term on the lattice site  $N$ .

There are only mass counterterms generated of the form  $\bar{\psi}_n \psi_n$ , and they are identical for all  $n$ . However, due to the different field strength renormalization of  $\psi_{LN}$ , the bare coupling  $v\eta$  of the term  $\bar{\psi}_N \psi_N$  in (4.24) must be assigned a different divergence in the course of renormalization. We have to conclude that the universality of couplings at all lattice sites is broken by quantum corrections. The Lagrangian of this deconstructed model is not renormalizable unless we allow for an independent mass parameter  $(v\eta)_N$ .

The divergent parts of the counterterms (4.49) imply a divergent shift of the renormalized parameters in the Lagrangian. The relation between bare and renormalized fields is given by

$$\psi_{L/Rn}^{\text{B}} = Z_{L/Rn}^{1/2} \psi_{L/Rn} \quad (4.50)$$

with

$$Z_{L/Rn}^{1/2} = 1 - \frac{1}{\epsilon} \frac{g^2}{32\pi^2} (\eta^2 + 1) \quad (4.51)$$

for all  $n$  except

$$Z_{LN}^{1/2} = 1 - \frac{1}{\epsilon} \frac{g^2}{32\pi^2}. \quad (4.52)$$

The shift in the mass matrix is then given by

$$\Delta \hat{M} = \hat{M} - \hat{M}^{\text{B}} = Z_L^{1/2} \hat{M}^{\text{B}} Z_R^{1/2} - \delta_{\hat{M}} - \hat{M}^{\text{B}}, \quad (4.53)$$

where we have written the field strength renormalization as diagonal matrices  $Z_{L/R}$ . The bare mass matrix (4.26) is here denoted by  $\hat{M}^{\text{B}}$  and the mass counterterm matrix by  $\delta_{\hat{M}}$ .

For the latter we find

$$\delta_{\hat{M}} = \frac{1}{\epsilon} \frac{g^2}{16\pi^2} 4v\eta \begin{pmatrix} 0 & 0 & 0 & \dots & 0 \\ 1 & 0 & 0 & \dots & 0 \\ 0 & 1 & 0 & \dots & 0 \\ \dots & \dots & \dots & \dots & \dots \\ 0 & \dots & 1 & 0 & \\ 0 & \dots & 0 & 1 & \end{pmatrix}. \quad (4.54)$$

There are no counterterms for the “off-diagonal” entries corresponding to the VEV of the linking Higgs. According to (4.53), the shift in the mass matrix is

$$\Delta\hat{M} = \frac{1}{\epsilon} \frac{g^2}{16\pi^2} v\eta \begin{pmatrix} -\eta^2 - 1 & 0 & 0 & \dots & 0 \\ \eta^2 - 3 & -\eta^2 - 1 & 0 & \dots & 0 \\ 0 & \eta^2 - 3 & -\eta^2 - 1 & \dots & 0 \\ \dots & \dots & \dots & \dots & \dots \\ 0 & \dots & \dots & \eta^2 - 3 & -\eta^2 - 1 \\ 0 & \dots & \dots & 0 & \frac{1}{2}\eta^2 - 3 \end{pmatrix}. \quad (4.55)$$

The “off-diagonal” entries proportional to  $-\eta^2 - 1$  are purely generated by the field strength renormalization.

If we ignore for a moment that the last entry in (4.55) is different from the other “diagonal” entries, the shift in the mass matrix is equivalent to a shift in the parameters

$$\Delta(v\eta) = \frac{1}{\epsilon} \frac{g^2}{16\pi^2} v\eta(-\eta^2 - 1), \quad (4.56)$$

$$\Delta\tilde{M} = \frac{1}{\epsilon} \frac{g^2}{16\pi^2} v\eta(\eta^2 - 3). \quad (4.57)$$

With  $\tilde{M} = M - v\eta$  this implies

$$\Delta M = -\frac{1}{\epsilon} \frac{g^2}{16\pi^2} 4v\eta. \quad (4.58)$$

Although we have set  $M = 0$  at tree level, radiative corrections induce a divergent shift  $\Delta M$ .

If we take the model as an effective theory valid up to a cut-off scale  $\Lambda$ , then (4.55) gives the running contribution to the mass matrix between the cut-off scale and a renormalization scale  $\tilde{\mu}$  via the replacement

$$\frac{1}{\epsilon} \longrightarrow \log \frac{\Lambda^2}{\tilde{\mu}^2}. \quad (4.59)$$

Expanding (4.30), the mass shift to one-loop order is given by

$$\Delta m_{\psi(k)} = [2\Delta(v\eta) - \Delta M] \sin \frac{k\pi}{2(N+1)}. \quad (4.60)$$

Inserting (4.56) and (4.58), and including the boundary contribution at the lattice site  $N$ , we find

$$\Delta m_{\psi(k)} = m_{\psi(k)} \frac{g^2}{16\pi^2} \log \frac{\Lambda^2}{\tilde{\mu}^2} \left[ -\eta^2 + 1 + \eta^2 \frac{1}{N+1} \cos^2 \frac{k\pi}{2(N+1)} \right]. \quad (4.61)$$

We see that the leading order mass shift is proportional to the tree-level mass. The boundary contribution, given by the last term in (4.61), vanishes in the limit  $N \rightarrow \infty$ , while the remaining part is actually zero, since we have set  $\eta = 1$  at tree-level.

The continuum limit is reached by taking  $a \rightarrow 0$  and  $N \rightarrow \infty$ , while keeping  $a(N+1) = \pi R$  fixed. In this limit

$$\Delta m_{\psi(k)} \rightarrow m_{\psi(k)} \frac{g_4^2}{16\pi^2} \log \frac{\Lambda^2}{\tilde{\mu}^2}, \quad (4.62)$$

where the 4-dimensional coupling  $g_4$  is given by

$$g^2 = \frac{2\pi R g_4^2}{2a}. \quad (4.63)$$

In comparison to the boundary contributions in the 5-dimensional orbifold model, equation (37) in [21], there is a difference of a factor 9/4 that is not reproduced here. Since the deconstructed setup differs from the continuum theory in the UV, it is not expected that they agree in the divergent parts of the self-energy. However, as we have already mentioned, these divergencies can be interpreted as the running contribution to the mass shift between the cut-off scale and the masses of the KK excitations, which turns out to be different here.

Moreover, equation (4.62) is only valid in the continuum limit. When taking dimensional deconstruction as a setup independent of the interpretation in terms of extra dimensions, we only have a finite number of lattice sites. This gives rise to additional differences according to (4.61), especially for low values of  $N$  which are not unrealistic for a cut-off scale in the TeV range. However, the numerical difference is quite small for the lowest KK modes.





# Chapter 5

## Conclusions

## 5.1 Conclusions

In this thesis we have investigated the extension of the Standard Model in universal extra dimensions. We presented the analysis of the decays  $B \rightarrow X_s \gamma$ ,  $B \rightarrow X_s$  gluon and  $B \rightarrow X_s \mu^+ \mu^-$  in the Appelquist, Cheng and Dobrescu (ACD) model with one universal extra dimension. In addition, we discussed Kaluza-Klein parity, renormalization and fermion mass corrections in the framework of dimensional deconstruction.

The decays  $B \rightarrow X_s$  gluon and  $B \rightarrow X_s \mu^+ \mu^-$  are calculated for the first time. The radiative decay  $B \rightarrow X_s \gamma$  has been considered in the past [4]. In contrast to that work, our analysis includes the numerically important NLO QCD corrections and a careful consideration of the experimental and theoretical uncertainties. Without them a reliable comparison between the SM, the ACD model and the experimental data would not be possible. As a byproduct, we generalize the background field method to five dimensions.

The calculated Inami-Lim functions also allow the analysis of the the decay  $K_L \rightarrow \pi^0 e^+ e^-$  and the CP-violating ratio  $\varepsilon'/\varepsilon$ . Unfortunately, these observables can presently not be used to constrain the parameter  $1/R$  of the ACD model due to either theoretical or experimental limitations. The same problems affect the SM analysis of these observables. However, the ACD model is fully consistent with the data within the theoretical and experimental uncertainties in these two observables [6].

The compactification radius  $1/R$  is the only additional parameter of the ACD model compared to the SM. For  $1/R = 300$  GeV, we observe the following interesting pattern:

The short distance function  $Z$ , relevant for  $B \rightarrow X_s \mu^+ \mu^-$ ,  $K_L \rightarrow \pi^0 e^+ e^-$  and  $\varepsilon'/\varepsilon$  is enhanced by 23% relative to the SM value. The functions  $D'$  and  $E'$ , relevant for  $B \rightarrow X_s \gamma$  and  $B \rightarrow X_s$  gluon are suppressed by 36% and 66%, respectively. The effects in the function  $D$  are negligible due to a cancellation of two contributions. The function  $E$  is moderately enhanced, which is, however, of no phenomenological relevance.

The branching ratio  $Br(B \rightarrow X_s \gamma)$  is suppressed by 20%. The phenomenological implications of this result depend sensitively on the value of  $m_c/m_b$  and on the experimental data. The lower bound on  $1/R$  is stronger for  $m_c/m_b=0.29$  than for  $m_c/m_b=0.22$ .

The branching ratio  $Br(B \rightarrow X_s$  gluon) is suppressed by 40%. At present, this result is phenomenologically not relevant. If, however, the large hadronic uncertainties can be reduced and the branching ratio can be extracted from the data, along with the reduction of the perturbative uncertainties, this observable will become relevant, since the impact of the KK modes is quite substantial.

In the decay  $B \rightarrow X_s \mu^+ \mu^-$  we observe an enhancement of the branching ratio of 12% and 16% for the low dilepton mass window and for the full spectrum, respectively. The zero in the forward-backward asymmetry  $\hat{s}_0$  in this decay provides an even more interesting test for the ACD model. The theoretical uncertainties are very small and the impact of the KK modes is quite large, shifting the zero from  $\hat{s}_0 = 0.162$  in the SM to  $\hat{s}_0 = 0.142$  in the ACD model.

These findings show that the ACD model is consistent with current experimental data for  $1/R \geq 300$  GeV. The results should also be compared with the ones obtained in the

analysis [3] of rare  $K$  and  $B$  decays. The value of  $1/R = 200$  GeV that was fully consistent with the decays considered there, is excluded by the decay  $B \rightarrow X_s \gamma$  which is suppressed relative to the SM by a factor of 1.6 at this low compactification scale. This is clearly excluded by the data. Unfortunately, the even stronger suppression of  $B \rightarrow X_s$  gluon cannot be used in this respect for the reasons explained above.

For a compactification scale of  $1/R = 300$  GeV, the following enhancements were found for the decays [3]:  $K^+ \rightarrow \pi^+ \nu \bar{\nu}$  (9%),  $K_L \rightarrow \pi^0 \nu \bar{\nu}$  (10%),  $B \rightarrow X_d \nu \bar{\nu}$  (12%),  $B \rightarrow X_s \nu \bar{\nu}$  (21%),  $K_L \rightarrow \mu \bar{\mu}$  (20%),  $B_d \rightarrow \mu \bar{\mu}$  (23%) and  $B_s \rightarrow \mu \bar{\mu}$  (33%). Combining these findings with the ones in this thesis, we observe that the main effects of the KK modes are felt in  $Z^0$ -penguins,  $\gamma$ -magnetic penguins and chromomagnetic penguins.

Compared to the SM, the ACD model is even closer to the central experimental values in the phenomenologically most relevant decays. The enhancement of the  $Z^0$ -penguins triggers an enhancement of the decay modes  $K^+ \rightarrow \pi^+ \nu \bar{\nu}$  and  $B \rightarrow X_s \mu^+ \mu^-$ . On the other hand, the experimental value for  $Br(B \rightarrow X_s \gamma)$  is presently below the SM expectation, and the suppression of the  $\gamma$ -magnetic penguins could also be welcome. However, in view of the present experimental and theoretical uncertainties, no definite conclusions can be drawn to prefer the ACD model over the SM.

Possibly, the most interesting result of this work is the sizable downward shift of the zero of the forward-backward asymmetry  $\hat{s}_0$  in the decay  $B \rightarrow X_s \mu^+ \mu^-$ . We emphasize that this shift has a definite sign and the theoretical uncertainties are small.

In this work we completed the study of the most interesting FCNC processes in the ACD model. The pattern of enhancements and suppressions relative to the SM predictions was determined as follows. There is an enhancement for  $K_L \rightarrow \pi^0 e^+ e^-$ ,  $\Delta M_s$ ,  $K^+ \rightarrow \pi^+ \nu \bar{\nu}$ ,  $K_L \rightarrow \pi^0 \nu \bar{\nu}$ ,  $B \rightarrow X_d \nu \bar{\nu}$ ,  $B \rightarrow X_s \nu \bar{\nu}$ ,  $K_L \rightarrow \mu^+ \mu^-$ ,  $B_d \rightarrow \mu^+ \mu^-$ ,  $B \rightarrow X_s \mu^+ \mu^-$  and  $B_s \rightarrow \mu^+ \mu^-$ , and a suppression for  $B \rightarrow X_s \gamma$ ,  $B \rightarrow X_s$  gluon, the value of  $\hat{s}_0$  in the forward-backward asymmetry of  $B \rightarrow X_s \mu^+ \mu^-$  and  $\varepsilon'/\varepsilon$ .

As we already pointed out, the predictions of the ACD model are generally closer to the central values of the experimental data. However, future experiments and better control of the theoretical uncertainties will show whether this pattern is required by the data or the ACD model with a low compactification scale of a few hundred GeV will be excluded. In the limit  $1/R \rightarrow \infty$ , all KK modes become infinitely massive and disappear from the spectrum, leaving only the particle content of the SM. Hence, there cannot be derived an *upper* limit on  $1/R$  without ruling out the SM at the same time.

Dimensional deconstruction is a way of introducing a gauge-invariant UV regulator in a higher dimensional theory, for example the ACD model. It also stands on its own right as a framework for building models that do not necessarily correspond in any way to extra dimensions. In the former case it is important that the deconstructed model agrees with the extra dimensional theory at low energies. This equivalence should comprise not only the mass spectrum but also the Feynman rules and important features like Kaluza-Klein parity conservation in UED models.

In this thesis we discussed the deconstructed aliphatic model of 5-dimensional QED with chiral fermions in the bulk. We show how to modify the Lagrangian and gauge fixing

from the non-chiral periodic case to apply to the aliphatic setup. The Feynman rules are shown to differ from the corresponding orbifold ones by terms violating KK parity.

We point out that due to the fermions in the bulk, there arise difficulties when using this setup as a UV completion of a UED model, since KK parity is no longer a symmetry of the Lagrangian. One reason is that the coupling of the fermions and gauge fields to the link fields induces a direction on the lattice. The other reason the realization of chiral zero-modes. In a deconstruction setup with chiral fermions in the bulk, this zero-mode is generated by asymmetric boundary conditions at the fixed points.

The issue of KK parity is not crucial for deconstructed models with fermions placed on unique lattice sites as opposed to the deconstructed UED model discussed in this thesis. For this reason dimensional deconstruction can in principle do a better job as a UV regulator for a higher dimensional model with fermions located at branes.

We emphasize that the origin of the fermion masses is twofold. It is given by the VEV of the link fields and by explicit mass terms. The tree level matching of the fermion mass spectrum requires a tuning of the parameters in the latter. We calculate the divergent part of the one-loop fermion self-energy and see that this structure is reflected here. Each Feynman diagram corresponds to a particular term in the Lagrangian and the required counterterms are easily identified. The divergencies differ for the two sets of fermion mass terms, substantiating the above naturalness problem. From the calculation of the fermion self-energy we also deduce the running contribution of the radiative corrections to the fermion mass spectrum. In the continuum limit our result differs by a factor  $9/4$  from the 5-dimensional orbifold model [21].

A peculiarity is the different field strength renormalization of the left-handed fermion at one endpoint of the lattice which induces a different renormalization of the associated mass parameter. We have to conclude that the universality of the couplings at all lattice sites is broken by quantum corrections. This is a consequence of the breaking of the “hopping” symmetry of the lattice at the endpoints, which is not the case in deconstructed compactifications on a circle. If one chooses the Lagrangian to possess a certain symmetry, like the universality of the couplings at all lattice sites, an explicit calculation must show if this symmetry is respected by quantum corrections. As the deconstructed model we consider is a gauge-invariant 4-dimensional theory with renormalizable operators, it is in principle renormalizable. However, this is only guaranteed if all parameters are taken to be independent.

In our calculation we find that at one-loop order only one lattice site requires a different infinite renormalization. It would be interesting to know whether other sites are affected in the same way by higher loop corrections. If this is the case, the parameters at all sites would have taken to be independent, and much of the predictability of the model would be lost. Setting equal the renormalized parameters by adjusting the counterterms by hand would imply fine-tuning and requires further motivation, for example the matching to a higher dimensional theory. Without such a reference, there is no general guiding principle for the choice of the parameters. However, dynamical realizations of non-universal couplings to generate curved geometries have been discussed in [19]. A

different approach was taken in [76], where the Lagrangian of the deconstructed theory is interpreted as the fixed point of a renormalization group transformation.



# Appendix A

## Background Field Method in 5 Dimensions

In order to calculate the functions  $D$ ,  $E$ ,  $D'$  and  $E'$ , we have used the method of background fields. The external particles are replaced by classical fields that do not need gauge fixing. This is necessary if one wants to calculate off-shell amplitudes while maintaining explicitly gauge invariance.

As in 1-PI diagrams the background fields only appear on the external legs, there is no need to fix the gauge for the background gauge fields. With the appropriate choice of the gauge fixing for the quantum gauge fields, we can ensure the invariance of the effective action with respect to background field (BF) gauge transformations. The general procedure in 4 dimensions is described in [37]. In this section we only state the SM case and modify the gauge fixing to fit the ACD model.

The starting point is the action  $S[\psi]$  before gauge fixing, where  $\psi$  denotes all gauge and matter fields in the action. We get the BF action by the transformation

$$S[\psi] \longrightarrow S[\psi + \hat{\psi}], \quad (\text{A.1})$$

where we have introduced the background fields  $\hat{\psi}$ . It is modified by the gauge fixing to

$$S_{\text{BF}}[\psi, \hat{\psi}] = S[\psi + \hat{\psi}] - \frac{1}{2\xi} \int d^d x \tilde{\mathcal{G}}\tilde{\mathcal{G}} + \text{ghost terms}, \quad (\text{A.2})$$

where  $\tilde{\mathcal{G}}\tilde{\mathcal{G}}$  stands for all gauge fixing functionals. As the terms with ghost fields are not relevant for us we will not consider them here.

In the 4-dimensional electroweak SM, a convenient choice for the gauge fixing functionals is

$$\tilde{\mathcal{G}}_{B,\text{SM}}[B, \phi, \hat{\phi}] = \partial_\mu B^\mu - ig'\xi \frac{1}{2} \left( \hat{\phi}^\dagger \phi - \phi^\dagger \hat{\phi} \right), \quad (\text{A.3})$$

$$\tilde{\mathcal{G}}_{A,\text{SM}}^a[A, \hat{A}, \phi, \hat{\phi}] = \partial_\mu A^{a\mu} + g_2 \epsilon^{abc} \hat{A}_\mu^b A^{c\mu} - ig_2 \xi \frac{1}{2} \left( \hat{\phi}^\dagger \sigma^a \phi - \phi^\dagger \sigma^a \hat{\phi} \right), \quad (\text{A.4})$$

with the Higgs fields

$$\hat{\phi} = \frac{1}{\sqrt{2}} \left( v + \hat{\psi} + i\hat{\chi}^a \sigma^a \right) \begin{pmatrix} 0 \\ 1 \end{pmatrix}, \quad \phi = \frac{1}{\sqrt{2}} (\psi + i\chi^a \sigma^a) \begin{pmatrix} 0 \\ 1 \end{pmatrix}, \quad (\text{A.5})$$

where  $\sigma^a$  are the common Pauli matrices. According to (A.2), the gauge fixing part of the Lagrangian is

$$\mathcal{L}_{\text{GF}} = -\frac{1}{2\xi} \tilde{\mathcal{G}}_B \tilde{\mathcal{G}}_B - \frac{1}{2\xi} \tilde{\mathcal{G}}_A^a \tilde{\mathcal{G}}_A^a. \quad (\text{A.6})$$

With this specific gauge fixing, the BF action is invariant under the BF gauge transformation<sup>1</sup>

$$\delta_{\text{BF}} \hat{B}_\mu = \frac{1}{g'} \partial_\mu \beta, \quad (\text{A.7})$$

$$\delta_{\text{BF}} \hat{A}_\mu^a = f^{abc} \hat{A}_\mu^b \alpha^c + \frac{1}{g_2} \partial_\mu \alpha^a, \quad (\text{A.8})$$

$$\delta_{\text{BF}} \hat{\phi} = i \left( \alpha^a \frac{\sigma^a}{2} + \frac{1}{2} \beta \right) \hat{\phi}, \quad (\text{A.9})$$

combined with a transformation of the quantum fields

$$\delta A_\mu^a = f^{abc} A_\mu^b \alpha^c, \quad (\text{A.10})$$

$$\delta \phi = i \left( \alpha^a \frac{\sigma^a}{2} + \frac{1}{2} \beta \right) \phi, \quad (\text{A.11})$$

where (A.10) and (A.11) are just unitary rotations in the functional integral.

The analogous BF gauge transformation in 5 dimensions is

$$\delta_{\text{BF}} \hat{B}_M = \frac{1}{\hat{g}'} \partial_M \beta, \quad (\text{A.12})$$

$$\delta_{\text{BF}} \hat{A}_M^a = f^{abc} \hat{A}_M^b \alpha^c + \frac{1}{\hat{g}_2} \partial_M \alpha^a, \quad (\text{A.13})$$

$$\delta_{\text{BF}} \hat{\phi} = i \left( \alpha^a \frac{\sigma^a}{2} + \frac{1}{2} \beta \right) \hat{\phi} \quad (\text{A.14})$$

combined with

$$\delta A_M^a = f^{abc} A_M^b \alpha^c, \quad (\text{A.15})$$

$$\delta \phi = i \left( \alpha^a \frac{\sigma^a}{2} + \frac{1}{2} \beta \right) \phi. \quad (\text{A.16})$$

---

<sup>1</sup>We omit the BF gauge transformation of the fermions which is just an ordinary gauge transformation.



Compared to 4 dimensions, the couplings  $g'$  and  $g_2$  have been replaced by their 5-dimensional analogs  $\hat{g}'$  and  $\hat{g}_2$ . All fields and  $\alpha^a$  and  $\beta$  are now also functions of the extra coordinate  $y$  and the vector index  $M$  can take the values  $M = 0, 1, 2, 3, 5$ .

In the ACD model, we have to add  $-\xi\partial_5 B_5$  to (A.3) and  $-\xi\partial_5 A_5^a$  to (A.4) in order to diagonalize the mass matrices of the bosonic modes [3]. However, this spoils BF gauge invariance, so we add another term to (A.4) to fix this and get

$$\tilde{\mathcal{G}}_{B,\text{ACD}}[B, \phi, \hat{\phi}] = \tilde{\mathcal{G}}_{B,\text{SM}}[B, \phi, \hat{\phi}] - \xi\partial_5 B_5, \quad (\text{A.17})$$

$$\tilde{\mathcal{G}}_{A,\text{ACD}}^a[A, \hat{A}, \phi, \hat{\phi}] = \tilde{\mathcal{G}}_{A,\text{SM}}^a[A, \hat{A}, \phi, \hat{\phi}] - \xi\partial_5 A_5^a - \xi\hat{g}_2\epsilon^{abc}\hat{A}_5^b A_5^c, \quad (\text{A.18})$$

where it is understood that  $g'$  and  $g_2$  have been replaced by  $\hat{g}'$  and  $\hat{g}_2$ .

The use of (A.17) and (A.18) ensures invariance of all 1-PI diagrams under BF gauge transformations in 5 dimensions. However, as we are only interested in external zero-mode fields, the last term in (A.18) does not affect our calculation.

In the diagrams for the calculation of the functions  $E$  and  $E'$ , the external gluon couples only to the quarks. As there are no fermions involved in the gauge fixing, the background gluon couples to quarks just like a quantum gluon, and there is no need to specify a gauge fixing functional for QCD. For completeness, we note that

$$\tilde{\mathcal{G}}_{G,\text{ACD}}^a[G, \hat{G}] = \partial_\mu G^{a\mu} + \hat{g}_s f^{abc} \hat{G}_\mu^b G^{c\mu} - \xi\partial_5 G_5^a - \xi\hat{g}_s f^{abc} \hat{G}_5^b G_5^c \quad (\text{A.19})$$

would be an appropriate choice. Here  $f^{abc}$  are the  $SU(3)_C$  structure constants and  $\hat{g}_s$  is the strong coupling constant.



# Appendix B

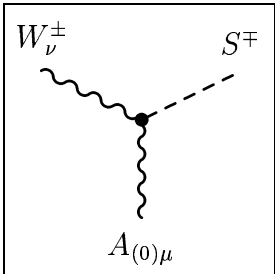
## Feynman Rules in the ACD Model: Photon and Gluons

In this section we list the Feynman rules needed for the calculations in this work except for those already given in [3]. The Feynman rules are derived in the 5d background field  $R_\xi$ -gauge described in Appendix A. The rules for vertices involving only quantum fields are the same as in the conventional 5d  $R_\xi$ -gauge described in [3].

In order to simplify the notation, we omit the KK indices of the fields. There is no ambiguity because in one-loop calculations at least one field is always a zero-mode. In the vertex rules given below, this is the photon  $A$ , the gluon  $G$  and their background equivalents. Due to KK parity conservation, the other two fields have equal KK mode number, i.e. either zero or  $n \geq 1$ .

Fermion zero-modes have substantially different Feynman rules than their KK excitations. The up-type quarks  $Q_i$  and  $U_i$  are always supposed to be ( $n \geq 1$ )-modes, while the zero-mode is labeled  $u$ . The generation index  $i$  can take the values  $i = u, c, t$ .

In the vertices below,  $S^\pm$  stands for the scalar modes  $G^\pm$  and  $a^\pm$ . All momenta and fields are assumed to be incoming. The Feynman rules for the vertices are:



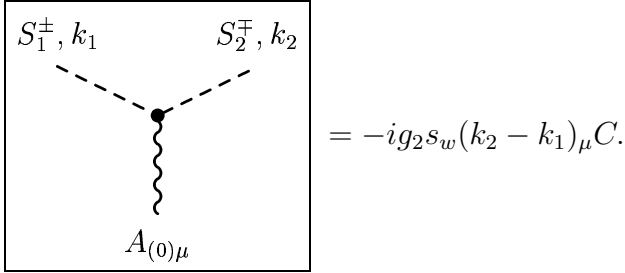
The diagram shows a vertex where a wavy line labeled  $W_\nu^\pm$  enters from the top left, a dashed line labeled  $S^\mp$  enters from the top right, and a wavy line labeled  $A_{(0)\mu}$  exits from the bottom. The vertex is represented by a black dot. To the right of the diagram is the equation  $= g_2 s_w M_{W(n)} g_{\mu\nu} C$ .

$$AW^+G^- : C = 1, \quad AW^-G^+ : C = -1, \quad (\text{B.1})$$

$$AW^+a^- : C = 0, \quad AW^-a^+ : C = 0, \quad (\text{B.2})$$

$$\hat{A}W^+G^- : C = 0, \quad \hat{A}W^-G^+ : C = 0, \quad (\text{B.3})$$

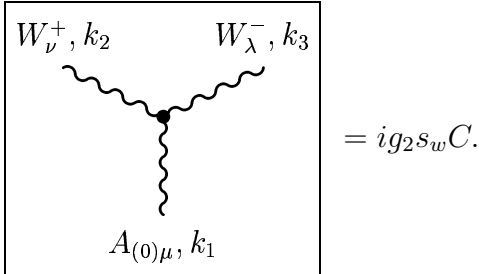
$$\hat{A}W^+a^- : C = 0, \quad \hat{A}W^-a^+ : C = 0. \quad (\text{B.4})$$



$$AG^+G^- : C = 1, \quad Aa^+a^- : C = 1, \quad (\text{B.5})$$

$$AG^+a^- : C = 0, \quad Aa^+G^- : C = 0, \quad (\text{B.6})$$

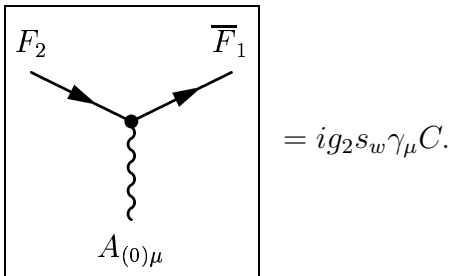
and the same values of  $C$  for the analogous vertices with a background photon  $\hat{A}$ .



$$AW^+W^- : C = g_{\mu\nu}(k_2 - k_1)_\lambda + g_{\mu\lambda}(k_1 - k_3)_\nu + g_{\lambda\nu}(k_3 - k_2)_\mu, \quad (\text{B.7})$$

$$\hat{A}W^+W^- : C = g_{\mu\nu}(k_2 - k_1 + \frac{1}{\xi}k_3)_\lambda + g_{\mu\lambda}(k_1 - k_3 - \frac{1}{\xi}k_2)_\nu \quad (\text{B.8})$$

$$+ g_{\lambda\nu}(k_3 - k_2)_\mu. \quad (\text{B.9})$$

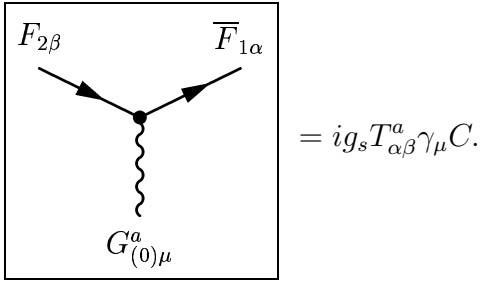


$$A\bar{u}_i u_i : C = \frac{2}{3}, \quad (\text{B.10})$$

$$A\bar{Q}_i Q_i : C = \frac{2}{3}, \quad A\bar{U}_i \mathcal{U}_i : C = \frac{2}{3}, \quad (\text{B.11})$$

$$A\bar{Q}_i \mathcal{U}_i : C = 0, \quad A\bar{U}_i Q_i : C = 0, \quad (\text{B.12})$$

and the same values of  $C$  for the analogous vertices with a background photon  $\hat{A}$ .



$$= ig_s T_{\alpha\beta}^a \gamma_\mu C.$$

$$G\bar{u}_i u_i : C = 1, \quad (\text{B.13})$$

$$G\bar{Q}_i Q_i : C = 1, \quad G\bar{U}_i \mathcal{U}_i : C = 1, \quad (\text{B.14})$$

$$G\bar{Q}_i \mathcal{U}_i : C = 0, \quad G\bar{U}_i Q_i : C = 0, \quad (\text{B.15})$$

and the same values of  $C$  for the analogous vertices with a background gluon  $\hat{G}$ .



# Appendix C

## Useful formulae

### C.1 Orthogonality relations

$$\sum_{n=1}^N \sin \frac{nk\pi}{N+1} \sin \frac{nl\pi}{N+1} = \begin{cases} 0 & \text{if } k = l = 0, \\ \frac{N+1}{2} \check{\delta}_{k-l} & \text{else,} \end{cases} \quad (\text{C.1})$$

where ( $n \in \mathbb{Z}$ )

$$\check{\delta}_j = \begin{cases} 1 & \text{if } j = 2n(N+1), \\ 0 & \text{else,} \end{cases} \quad (\text{C.2})$$

not to be confused with  $\hat{\delta}_j$  as defined in (4.40).

$$\sum_{k=0}^N \left(\frac{1}{2}\right)^{\delta_k} \cos \frac{(n+1/2)k\pi}{N+1} \cos \frac{(n'+1/2)k\pi}{N+1} = \frac{N+1}{2} \check{\delta}_{n-n'}. \quad (\text{C.3})$$

$$\left(\frac{1}{\sqrt{2}}\right)^{\delta_k+\delta_l} \sum_{n=0}^N \cos \frac{(n+1/2)k\pi}{N+1} \cos \frac{(n+1/2)l\pi}{N+1} = \frac{N+1}{2} \check{\delta}_{k-l}. \quad (\text{C.4})$$

### C.2 Vertex sums

$$\Xi(j) \equiv \sum_{n=1}^N \sin \frac{nj\pi}{N+1} = \sin \frac{Nj\pi}{2(N+1)} \sin \frac{j\pi}{2} \sin^{-1} \frac{j\pi}{2(N+1)}. \quad (\text{C.5})$$

For integer  $j$  this can be written as

$$\Xi(j) = \omega(j) \cos \frac{j\pi}{2(N+1)} \sin^{-1} \frac{j\pi}{2(N+1)} \quad (\text{C.6})$$

with

$$\omega(j) = \begin{cases} 1 & \text{if } j \text{ is odd,} \\ 0 & \text{if } j \text{ is even.} \end{cases} \quad (\text{C.7})$$

$$\Omega(j) \equiv \sum_{n=0}^N \cos \frac{nj\pi}{N+1} = \cos \frac{Nj\pi}{2(N+1)} \sin \frac{j\pi}{2} \sin^{-1} \frac{j\pi}{2(N+1)}. \quad (\text{C.8})$$

For integer  $j$  this can be written as

$$\Omega(j) = (N+1)\check{\delta}_j + \omega(j). \quad (\text{C.9})$$

### C.3 Sum in the $\bar{\psi}_L \mathcal{A} \psi_L$ vertex

Here we give the derivation of the coupling of the gauge field to the left-handed fermions in (4.38). First we note that

$$\begin{aligned} \sum_{n=0}^N \cos \frac{(n+1/2)j\pi}{N+1} &= \sum_{n=0}^N \left[ \cos \frac{nj\pi}{N+1} \cos \frac{j\pi}{2(N+1)} - \sin \frac{nj\pi}{N+1} \sin \frac{j\pi}{2(N+1)} \right] \\ &= \left[ \left( (N+1)\check{\delta}_j + \omega(j) \right) \cos \frac{j\pi}{2(N+1)} - \omega(j) \cos \frac{j\pi}{2(N+1)} \right] \\ &= (N+1)\check{\delta}_j \cos \frac{j\pi}{2(N+1)} = (N+1)\hat{\delta}_j, \end{aligned} \quad (\text{C.10})$$

where we have used (C.6) and (C.9), and  $\hat{\delta}_j$  is defined in (4.40). With the help of (C.10) we can easily evaluate the sum

$$\begin{aligned} &\sum_{n=0}^N \cos \frac{(n+1/2)k\pi}{N+1} \cos \frac{(n+1/2)l\pi}{N+1} \cos \frac{(n+1/2)m\pi}{N+1} \\ &= \frac{1}{4} \sum_{n=0}^N \left[ \cos \frac{(n+1/2)(k+l-m)\pi}{N+1} + \cos \frac{(n+1/2)(-k+l+m)\pi}{N+1} \right. \\ &\quad \left. + \cos \frac{(n+1/2)(k-l+m)\pi}{N+1} + \cos \frac{(n+1/2)(k+l+m)\pi}{N+1} \right] \\ &= \frac{N+1}{4} \hat{\delta}_{klm}, \end{aligned} \quad (\text{C.11})$$

where  $\hat{\delta}_{klm}$  is given by (4.39).



# Appendix D

## Fermion self-energy

Here we give the calculation of the Fermion self-energy diagrams in Fig. 4.4 in 't Hooft Feynman gauge ( $\xi = 1$ ). The 4D loop integrals were regularized dimensionally with  $d = 4 - 2\epsilon$ . As an example, we evaluate the first diagram of Fig. 4.4 with the scalar  $G$  running in the loop. The incoming (outgoing) state is labeled by the KK index  $k$  ( $k'$ ), and the fermion (boson) in the loop by the index  $l$  ( $m$ ). There is only a contribution proportional to  $\not{p}$ . For given mode numbers  $k, k', l$  and  $m$  the amplitude reads

$$\begin{aligned}
 -i\Sigma_{(S)}^{(1)l,m} &= \frac{1}{\epsilon} \frac{ig^2\eta^2}{16\pi^2} \frac{1}{4} \not{p}(1 + \gamma_5) \left( \frac{2}{N+1} \right)^3 \sum_{n,n'=1}^N \sin \frac{nk\pi}{N+1} \sin \frac{n'k'\pi}{N+1} \\
 &\times \left( \frac{1}{2} \right)^{\delta_l} \cos \frac{(n-1/2)l\pi}{N+1} \cos \frac{(n'-1/2)l\pi}{N+1} \sin \frac{nm\pi}{N+1} \sin \frac{n'm\pi}{N+1}. \quad (\text{D.1})
 \end{aligned}$$

The full amplitude is given by the sum of (D.1) over the internal KK mode numbers  $l$  and  $m$ . We can interchange the summation over the mode numbers with the summation over the lattice sites  $n$  and  $n'$ . The calculation of the diagram would be much more laborious if we used expressions for the vertices where the sum over the lattice sites is already evaluated. Moreover, we get the result in a form that is very convenient for us, namely with one remaining sum over lattice sites.

The result for this particular diagram is

$$-i\Sigma_{(S)}^{(1)} = \frac{1}{\epsilon} \frac{ig^2\eta^2}{16\pi^2} \frac{1}{4} \not{p}(1 + \gamma_5) \frac{2}{N+1} \sum_{n=1}^N \sin \frac{nk\pi}{N+1} \sin \frac{nk'\pi}{N+1}. \quad (\text{D.2})$$

The other diagrams are evaluated in a similar manner. The diagrams (5)-(8) depend on the mass of the fermion in the loop. Since the dependence is linear in the mass, there is simply a factor of  $m_{(l)} = 2v\eta \sin(l\pi/2(N+1))$  included in the summation over mode numbers.

The results for all diagrams in Fig. 4.4 are

$$-i\Sigma_{(S)}^{(1)} = \frac{1}{\epsilon} \frac{ig^2\eta^2}{32\pi^2} \frac{2}{N+1} \sum_{n=1}^N \sin \frac{nk\pi}{N+1} \sin \frac{nk'\pi}{N+1} \not{p} P_R, \quad (\text{D.3})$$

$$-i\Sigma_{(V)}^{(2)} = \frac{1}{\epsilon} \frac{ig^2}{16\pi^2} \frac{2}{N+1} \sum_{n=1}^N \sin \frac{nk\pi}{N+1} \sin \frac{nk'\pi}{N+1} \not{p} P_R, \quad (\text{D.4})$$

$$-i\Sigma_{(S)}^{(3)} = \frac{1}{\epsilon} \frac{ig^2\eta^2}{32\pi^2} \frac{2}{N+1} \left( \frac{1}{\sqrt{2}} \right)^{\delta_k + \delta_{k'}} \sum_{n=0}^{N-1} \cos \frac{(n+1/2)k\pi}{N+1} \cos \frac{(n+1/2)k'\pi}{N+1} \not{p} P_L, \quad (\text{D.5})$$

$$-i\Sigma_{(V)}^{(4)} = \frac{1}{\epsilon} \frac{ig^2}{16\pi^2} \frac{2}{N+1} \left( \frac{1}{\sqrt{2}} \right)^{\delta_k + \delta_{k'}} \sum_{n=0}^N \cos \frac{(n+1/2)k\pi}{N+1} \cos \frac{(n+1/2)k'\pi}{N+1} \not{p} P_L, \quad (\text{D.6})$$

$$-i\Sigma_{(S)}^{(5)} = -\frac{1}{\epsilon} \frac{ig^2\eta^2}{16\pi^2} v\eta \frac{2}{N+1} \left( \frac{1}{\sqrt{2}} \right)^{\delta_{k'}} \sum_{n=1}^N \sin \frac{nk\pi}{N+1} \cos \frac{(n-1/2)k'\pi}{N+1} P_R, \quad (\text{D.7})$$

$$-i\Sigma_{(V)}^{(6)} = \frac{1}{\epsilon} \frac{ig^2}{16\pi^2} 4v\eta \frac{2}{N+1} \left( \frac{1}{\sqrt{2}} \right)^{\delta_{k'}} \sum_{n=1}^N \sin \frac{nk\pi}{N+1} \cos \frac{(n+1/2)k'\pi}{N+1} P_R, \quad (\text{D.8})$$

$$-i\Sigma_{(S)}^{(7)} = -\frac{1}{\epsilon} \frac{ig^2\eta^2}{16\pi^2} v\eta \frac{2}{N+1} \left( \frac{1}{\sqrt{2}} \right)^{\delta_k} \sum_{n=1}^N \cos \frac{(n-1/2)k\pi}{N+1} \sin \frac{nk'\pi}{N+1} P_L, \quad (\text{D.9})$$

$$-i\Sigma_{(V)}^{(8)} = \frac{1}{\epsilon} \frac{ig^2}{16\pi^2} 4v\eta \frac{2}{N+1} \left( \frac{1}{\sqrt{2}} \right)^{\delta_k} \sum_{n=1}^N \cos \frac{(n+1/2)k\pi}{N+1} \sin \frac{nk'\pi}{N+1} P_L. \quad (\text{D.10})$$

Note that the mass of the boson in the loop does not enter the divergent part of the self-energy, and thus we cannot ignore the possibly very heavy fields  $\Sigma$ . The scalar amplitudes above are given for the Goldstone modes  $G$  running in the loop. The physical scalars  $\Sigma$  gives the same contributions but with different sign for diagrams (5) and (7). This is due to charge conservation, and consequently these two contributions cancel.

The sums in (D.3), (D.4) and (D.6) are given by the orthogonality relations (C.1) and (C.4). We can write, for example for (D.3),

$$-i\Sigma_{(S)}^{(1)} = \frac{1}{\epsilon} \frac{ig^2\eta^2}{32\pi^2} \delta_{k-k'} \not{p} P_R. \quad (\text{D.11})$$

This does not work for (D.5), since there the sum runs only from 0 to  $N-1$ . The reason is that the two vertices in the corresponding diagram are given by a sum over only  $N$  lattice sites. Moreover, the finite contributions will in general include transitions between arbitrary KK levels for all diagrams.

The amplitudes (D.3) - (D.10) can be readily converted into position space on the lattice. Remembering that the amplitudes describe transitions between arbitrary modes  $k$  and  $k'$  and comparing with the mode expansion of the fermions (4.27), we can write

$$-i\Sigma_{(S)}^{(1)} \sim \frac{1}{\epsilon} \frac{ig^2\eta^2}{32\pi^2} \sum_{n=1}^N \bar{\psi}_{Rn} \not{p} \psi_{Rn}, \quad -i\Sigma_{(V)}^{(2)} \sim \frac{1}{\epsilon} \frac{ig^2}{16\pi^2} \sum_{n=1}^N \bar{\psi}_{Rn} \not{p} \psi_{Rn}, \quad (\text{D.12})$$

$$-i\Sigma_{(S)}^{(3)} \sim \frac{1}{\epsilon} \frac{ig^2\eta^2}{32\pi^2} \sum_{n=0}^{N-1} \bar{\psi}_{Ln} \not{p} \psi_{Ln}, \quad -i\Sigma_{(V)}^{(4)} \sim \frac{1}{\epsilon} \frac{ig^2}{16\pi^2} \sum_{n=0}^N \bar{\psi}_{Ln} \not{p} \psi_{Ln}, \quad (\text{D.13})$$

$$-i\Sigma_{(S)}^{(5)} \sim -\frac{1}{\epsilon} \frac{ig^2\eta^2}{16\pi^2} v\eta \sum_{n=1}^N \bar{\psi}_{Ln-1} \psi_{Rn}, \quad -i\Sigma_{(V)}^{(6)} \sim \frac{1}{\epsilon} \frac{ig^2}{16\pi^2} 4v\eta \sum_{n=1}^N \bar{\psi}_{Ln} \psi_{Rn}, \quad (\text{D.14})$$

$$-i\Sigma_{(S)}^{(7)} \sim -\frac{1}{\epsilon} \frac{ig^2\eta^2}{16\pi^2} v\eta \sum_{n=1}^N \bar{\psi}_{Rn} \psi_{Ln-1}, \quad -i\Sigma_{(V)}^{(8)} \sim \frac{1}{\epsilon} \frac{ig^2}{16\pi^2} 4v\eta \sum_{n=1}^N \bar{\psi}_{Rn} \psi_{Ln}. \quad (\text{D.15})$$

We see that each diagram corresponds to a particular term in the Lagrangian. Including the appropriate factors for the scalar diagrams as discussed above, we can directly read off the counterterms. The incomplete sum in the first relation in (D.13) induces an extra contribution to the counterterm on the lattice site  $N$ .



# Bibliography

- [1] I. Antoniadis, Phys. Lett. B **246** (1990) 377; I. Antoniadis, C. Munoz and M. Quiros, Nucl. Phys. B **397** (1993) 515 [arXiv:hep-ph/9211309]; I. Antoniadis and K. Benakli, Phys. Lett. B **326** (1994) 69 [arXiv:hep-th/9310151]; I. Antoniadis, K. Benakli and M. Quiros, Phys. Lett. B **331** (1994) 313 [arXiv:hep-ph/9403290].
- [2] T. Appelquist, H. C. Cheng and B. A. Dobrescu, Phys. Rev. D **64** (2001) 035002 [arXiv:hep-ph/0012100].
- [3] A. J. Buras, M. Spranger and A. Weiler, Nucl. Phys. B **660** (2003) 225 [arXiv:hep-ph/0212143].
- [4] K. Agashe, N. G. Deshpande and G. H. Wu, Phys. Lett. B **514** (2001) 309 [arXiv:hep-ph/0105084].
- [5] A. Alavi-Harati *et al.* [KTeV Collaboration], Phys. Rev. Lett. **93** (2004) 021805 [arXiv:hep-ex/0309072].
- [6] A. J. Buras, A. Poschenrieder, M. Spranger and A. Weiler, Nucl. Phys. B **678** (2004) 455 [arXiv:hep-ph/0306158].
- [7] T. Appelquist and H. U. Yee, Phys. Rev. D **67** (2003) 055002 [arXiv:hep-ph/0211023].
- [8] P. Bucci and B. Grzadkowski, arXiv:hep-ph/0304121.
- [9] K. Agashe, N. G. Deshpande and G. H. Wu, Phys. Lett. B **511** (2001) 85, [arXiv:hep-ph/0103235]; T. Appelquist and B. A. Dobrescu, Phys. Lett. B **516** (2001) 85, [arXiv:hep-ph/0106140].
- [10] J. F. Oliver, J. Papavassiliou and A. Santamaria, Phys. Rev. D **67** (2003) 056002 [arXiv:hep-ph/0212391].
- [11] N. Arkani-Hamed, A. G. Cohen and H. Georgi, Phys. Rev. Lett. **86**, 4757 (2001) [arXiv:hep-th/0104005].
- [12] C. T. Hill, S. Pokorski and J. Wang, Phys. Rev. D **64** (2001) 105005 [arXiv:hep-th/0104035].

- 
- [13] D. M. Ghilencea, Phys. Rev. D **70** (2004) 045011 [arXiv:hep-th/0311187].
- [14] S. Nojiri, S. D. Odintsov and A. Sugamoto, Phys. Lett. B **590**, 239 (2004) [arXiv:hep-th/0401203]. H. C. Cheng, C. T. Hill and J. Wang, Phys. Rev. D **64**, 095003 (2001) [arXiv:hep-ph/0105323]. N. Arkani-Hamed, A. G. Cohen and H. Georgi, Phys. Lett. B **513**, 232 (2001) [arXiv:hep-ph/0105239].
- [15] C. Csaki, G. D. Kribs and J. Terning, Phys. Rev. D **65**, 015004 (2002) [arXiv:hep-ph/0107266]. H. C. Cheng, K. T. Matchev and J. Wang, Phys. Lett. B **521**, 308 (2001) [arXiv:hep-ph/0107268]. P. H. Chankowski, A. Falkowski and S. Pokorski, JHEP **0208**, 003 (2002) [arXiv:hep-ph/0109272]. T. j. Li and T. Liu, Eur. Phys. J. C **28**, 545 (2003) [arXiv:hep-th/0204128].
- [16] J. Giedt, E. Poppitz and M. Rozali, JHEP **0303** (2003) 035 [arXiv:hep-th/0301048]. E. Dudas, A. Falkowski and S. Pokorski, Phys. Lett. B **568**, 281 (2003) [arXiv:hep-th/0303155]. S. Chang and H. Georgi, Nucl. Phys. B **672**, 101 (2003) [arXiv:hep-th/0209038].
- [17] N. Arkani-Hamed, H. Georgi and M. D. Schwartz, Annals Phys. **305**, 96 (2003) [arXiv:hep-th/0210184]. N. Arkani-Hamed and M. D. Schwartz, Phys. Rev. D **69**, 104001 (2004) [arXiv:hep-th/0302110]. M. Bander, Phys. Rev. D **64**, 105021 (2001) [arXiv:hep-th/0107130].
- [18] K. Sfetsos, Nucl. Phys. B **612** (2001) 191 [arXiv:hep-th/0106126]. A. Falkowski and H. D. Kim, JHEP **0208** (2002) 052 [arXiv:hep-ph/0208058]. L. Randall, Y. Shadmi and N. Weiner, JHEP **0301** (2003) 055 [arXiv:hep-th/0208120]. A. Katz and Y. Shadmi, arXiv:hep-th/0409223.
- [19] H. Abe, T. Kobayashi, N. Maru and K. Yoshioka, Phys. Rev. D **67** (2003) 045019 [arXiv:hep-ph/0205344].
- [20] C. T. Hill, Phys. Rev. Lett. **88** (2002) 041601 [arXiv:hep-th/0109068]. I. Rothstein and W. Skiba, Phys. Rev. D **65**, 065002 (2002) [arXiv:hep-th/0109175]. N. Arkani-Hamed, A. G. Cohen, D. B. Kaplan, A. Karch and L. Motl, JHEP **0301**, 083 (2003) [arXiv:hep-th/0110146]. W. Skiba and D. Smith, Phys. Rev. D **65**, 095002 (2002) [arXiv:hep-ph/0201056]. R. S. Chivukula and H. J. He, Phys. Lett. B **532** (2002) 121 [arXiv:hep-ph/0201164]. Z. Berezhiani, A. Gorsky and I. I. Kogan, JETP Lett. **75**, 530 (2002) [Pisma Zh. Eksp. Teor. Fiz. **75**, 646 (2002)] [arXiv:hep-th/0203016]. N. Arkani-Hamed, A. G. Cohen, E. Katz, A. E. Nelson, T. Gregoire and J. G. Wacker, JHEP **0208**, 021 (2002) [arXiv:hep-ph/0206020]. C. Csaki, J. Erlich and J. Terning, Phys. Rev. D **67** (2003) 025019 [arXiv:hep-th/0208095]. P. Brax, R. A. Janik and R. Peschanski, Nucl. Phys. B **660**, 194 (2003) [arXiv:hep-th/0303081]. K. R. S. Balaji, M. Lindner and G. Seidl, Phys. Rev. Lett. **91**, 161803 (2003) [arXiv:hep-ph/0303245]. D. T. Son and M. A. Stephanov, Phys. Rev. D **69**, 065020 (2004) [arXiv:hep-ph/0304182]. E. Poppitz, JHEP **0308**, 044 (2003) [arXiv:hep-th/0306204]. F. Bauer,

- M. Lindner and G. Seidl, JHEP **0405**, 026 (2004) [arXiv:hep-th/0309200]. R. Casalbuoni, S. De Curtis and D. Dominici, arXiv:hep-ph/0405188.
- [21] H. C. Cheng, K. T. Matchev and M. Schmaltz, Phys. Rev. D **66** (2002) 036005 [arXiv:hep-ph/0204342]. M. Puchwein and Z. Kunszt, Annals Phys. **311** (2004) 288 [arXiv:hep-th/0309069].
- [22] Z. Kunszt, A. Nyffeler and M. Puchwein, JHEP **0403** (2004) 061 [arXiv:hep-ph/0402269].
- [23] A. Falkowski, C. Grojean and S. Pokorski, Phys. Lett. B **535** (2002) 258 [arXiv:hep-ph/0203033].
- [24] N. Maru and K. Yoshioka, Eur. Phys. J. C **31**, 245 (2003) [arXiv:hep-ph/0311337].
- [25] A. Falkowski, C. Grojean and S. Pokorski, Phys. Lett. B **581**, 236 (2004) [arXiv:hep-ph/0310201].
- [26] H. Georgi, A. K. Grant and G. Hailu, Phys. Lett. B **506** (2001) 207 [arXiv:hep-ph/0012379].
- [27] T. Appelquist and J. Carazzone, Phys. Rev. D **11** (1975) 2856.
- [28] H. Georgi and H. D. Politzer, Phys. Rev. D **14**, 1829 (1976).
- [29] F. Jegerlehner, Eur. Phys. J. C **18** (2001) 673 [arXiv:hep-th/0005255].
- [30] S. Chandrasekharan and U. J. Wiese, Prog. Part. Nucl. Phys. **53** (2004) 373 [arXiv:hep-lat/0405024].
- [31] G. 't Hooft and M. J. G. Veltman, Nucl. Phys. B **44** (1972) 189, P. Breitenlohner and D. Maison, Commun. Math. Phys. **52** (1977) 11, P. Breitenlohner and D. Maison, Commun. Math. Phys. **52** (1977) 39, P. Breitenlohner and D. Maison, Commun. Math. Phys. **52** (1977) 55, D. A. Akyeampong and R. Delbourgo, Nuovo Cim. A **17** (1973) 578, D. A. Akyeampong and R. Delbourgo, Nuovo Cim. A **18** (1973) 94, D. A. Akyeampong and R. Delbourgo, Nuovo Cim. A **19** (1974) 219.
- [32] A. Denner, Fortsch. Phys. **41** (1993) 307.
- [33] P. Gambino, P. A. Grassi and F. Madricardo, Phys. Lett. B **454**, 98 (1999) [arXiv:hep-ph/9811470].
- [34] T. Inami and C.S. Lim, Progr. Theor. Phys. **65** (1981) 297.
- [35] G. Buchalla and A.J. Buras, Nucl. Phys. B **398** (1993) 285.
- [36] C. Bobeth, M. Misiak and J. Urban, Nucl. Phys. B **574** (2000) 291 [arXiv:hep-ph/9910220].

- 
- [37] L. F. Abbott, Nucl. Phys. B **185** (1981) 189; L. F. Abbott, Acta Phys. Polon. B **13** (1982) 33; L. F. Abbott, M. T. Grisaru and R. K. Schaefer, Nucl. Phys. B **229** (1983) 372.
- [38] S. Wolfram, The MATHEMATICA book, Fourth Edition, Wolfram Media/Cambridge University Press, Champaign/Melbourne 1999.
- [39] A. Poschenrieder, Diploma Thesis.
- [40] G. Buchalla, A.J. Buras and M.K. Harlander, Nucl. Phys. B **349** (1991) 1.
- [41] D. Chakraverty, K. Huitu and A. Kundu, Phys. Lett. B **558** (2003) 173 [arXiv:hep-ph/0212047].
- [42] A.J. Buras, hep-ph/9806471, in *Probing the Standard Model of Particle Interactions*, eds. R. Gupta, A. Morel, E. de Rafael and F. David (Elsevier Science B.V., Amsterdam, 1998), page 281.
- [43] A. J. Buras, M. Misiak, M. Münz and S. Pokorski, Nucl. Phys. B **424** (1994) 374.
- [44] S. Bertolini, F. Borzumati and A. Masiero, Phys. Rev. Lett. **59** (1987) 180.
- [45] N. G. Deshpande, P. Lo, J. Trampetic, G. Eilam and P. Singer Phys. Rev. Lett. **59** (1987) 183.
- [46] M. Battaglia *et al.*, arXiv:hep-ph/0304132.
- [47] Heavy Flavor Averaging Group (HFAG), <http://www.slac.stanford.edu/xorg/hfag/rare/lep-ph05/rad11/index.html>
- [48] P. Gambino and M. Misiak, Nucl. Phys. B **611** (2001) 338 [arXiv:hep-ph/0104034].
- [49] A. J. Buras, A. Czarnecki, M. Misiak and J. Urban, Nucl. Phys. B **631** (2002) 219 [arXiv:hep-ph/0203135].
- [50] P. Gambino and U. Haisch, JHEP **0009** (2000) 001 [arXiv:hep-ph/0007259], P. Gambino and U. Haisch, JHEP **0110** (2001) 020 [arXiv:hep-ph/0109058].
- [51] A. J. Buras and M. Misiak, Acta Phys. Polon. B **33** (2002) 2597 [arXiv:hep-ph/0207131].
- [52] A. Ali and M. Misiak in [46].
- [53] T. Hurth, arXiv:hep-ph/0212304.
- [54] C. Greub and P. Liniger, Phys. Lett. B **494** (2000) 237 [arXiv:hep-ph/0008071]; C. Greub and P. Liniger, Phys. Lett. B **494** (2000) 237 [arXiv:hep-ph/0008071].



- [55] H. H. Asatrian, H. M. Asatrian, C. Greub and M. Walker, Phys. Lett. B **507** (2001) 162 [arXiv:hep-ph/0103087]; H. H. Asatryan, H. M. Asatrian, C. Greub and M. Walker, Phys. Rev. D **65** (2002) 074004 [arXiv:hep-ph/0109140]; H. H. Asatryan, H. M. Asatrian, C. Greub and M. Walker, Phys. Rev. D **66** (2002) 034009 [arXiv:hep-ph/0204341]; H. M. Asatrian, K. Bieri, C. Greub and A. Hovhannisyanyan, Phys. Rev. D **66** (2002) 094013 [arXiv:hep-ph/0209006].
- [56] A. Ghinculov, T. Hurth, G. Isidori and Y. P. Yao, Nucl. Phys. B **648** (2003) 254 [arXiv:hep-ph/0208088]; A. Ghinculov, T. Hurth, G. Isidori and Y. P. Yao, arXiv:hep-ph/0211197.
- [57] P. Gambino, M. Gorbahn and U. Haisch, Nucl. Phys. B **673**, 238 (2003) [arXiv:hep-ph/0306079]. C. Bobeth, P. Gambino, M. Gorbahn and U. Haisch, JHEP **0404** (2004) 071 [arXiv:hep-ph/0312090].
- [58] B. Aubert *et al.* [BABAR Collaboration], Phys. Rev. Lett. **93** (2004) 081802 [arXiv:hep-ex/0404006].
- [59] K. Abe *et al.* [Belle Collaboration], arXiv:hep-ex/0408119.
- [60] J. Kaneko *et al.* [Belle Collaboration], Phys. Rev. Lett. **90** (2003) 021801 [arXiv:hep-ex/0208029].
- [61] A. Ali, E. Lunghi, C. Greub and G. Hiller, Phys. Rev. D **66** (2002) 034002 [arXiv:hep-ph/0112300].
- [62] A. Ali, T. Mannel and T. Morozumi, Phys. Lett. **B273** (1991) 505.
- [63] M. Misiak, Nucl. Phys. **B393** (1993) 23; Erratum, Nucl. Phys. **B439** (1995) 461.
- [64] A.J. Buras and M. Münz, Phys. Rev. D **52** (1995) 186.
- [65] G. Burdman, Phys. Rev. D **57** (1998) 4254.
- [66] H. C. Cheng, C. T. Hill, S. Pokorski and J. Wang, Phys. Rev. D **64** (2001) 065007 [arXiv:hep-th/0104179].
- [67] C. Csaki, J. Erlich, V. V. Khoze, E. Poppitz, Y. Shadmi and Y. Shirman, Phys. Rev. D **65** (2002) 085033 [arXiv:hep-th/0110188].
- [68] N. Arkani-Hamed, A. G. Cohen and H. Georgi, JHEP **0207**, 020 (2002) [arXiv:hep-th/0109082].
- [69] H. Georgi, A. K. Grant and G. Hailu, Phys. Rev. D **63** (2001) 064027 [arXiv:hep-ph/0007350].
- [70] A. Falkowski, H. P. Nilles, M. Olechowski and S. Pokorski, Phys. Lett. B **566** (2003) 248 [arXiv:hep-th/0212206].

- [71] C. T. Hill and A. K. Leibovich, Phys. Rev. D **66** (2002) 016006 [arXiv:hep-ph/0205057].
- [72] G. Servant and T. M. Tait, [arXiv:hep-ph/0206071]. H. C. Cheng, J. L. Feng and K. T. Matchev, [arXiv:hep-ph/0207125]; D. Hooper and G. D. Kribs, [arXiv:hep-ph/0208261]; G. Servant and T. M. Tait, [arXiv:hep-ph/0209262]; D. Majumdar, [arXiv:hep-ph/0209277].
- [73] J. Papavassiliou and A. Santamaria, Phys. Rev. D **63**, 016002 (2001) [arXiv:hep-ph/0008151]. J. F. Oliver, J. Papavassiliou and A. Santamaria, Nucl. Phys. Proc. Suppl. **120**, 210 (2003) [arXiv:hep-ph/0209021].
- [74] A. J. Buras, A. Poschenrieder, M. Spranger and A. Weiler, eConf **C0304052**, WG302 (2003) [arXiv:hep-ph/0307202].
- [75] I. S. Gradshteyn and I. M. Ryzhik, “Table of Integrals, Series, and Products”, Academic Press, fifth edition (1994).
- [76] C. T. Hill, arXiv:hep-th/0303267.

# Acknowledgments

First of all I want to thank my advisor, Prof. Andrzej Buras, for providing me with the opportunity of working in his group. As his collaborator, I was able to learn from his profound knowledge of the subject and his deep insights. I am grateful for his valuable advice, encouragement, patience and personal support throughout the years.

Next I want to thank Prof. Wolfgang Hollik and the Max-Planck-Institut für Physik (Werner Heisenberg Institut) for providing me with financial support and the opportunity to participate in their community.

I particularly want to thank my collaborators Andreas Weiler and Anton Poschenrieder. I always very much enjoyed the amicable and fruitful atmosphere of our collaboration and the numerous valuable discussions we had on physics and beyond.

I would like to thank my four roommates during the years, Christoph Bobeth, Dominik Bauer, Michael Wick and Pavel Fileviez Perez for the relaxed and stimulating atmosphere in our common office that I was fortunate to experience with each one of them. I very much appreciated the numerous discussions, chats and social activities I had with the members of the physics department at the TUM. My thanks go to Rouzbeh Allahverdi, Cyrille Barbot, Monika Blanke, Robert Buras, Emily Clark, Thorsten Ewerth, Laura Fabietti, Benedikt Gaißmaier, Martin Gorbahn, Claudia Hagedorn, Uli Haisch, Sebastian Jäger, Jörn Kersten, Frank Krüger, Rita de Masi, Markus Michael Müller, Kin-ya Oda, Stefan Recksiegel, Dominik Streibl, Selma Uhlig, Andreas Weinberger and Elmar Wyszomirski. Special thanks go to Marc-Thomas Eisele, Mark "Marc" Rolinec, Felix Schwab and Jörg Urban for all the much valued discussions on physics, life, and everything else.

Many thanks go to Elke Krüger, Karin Ramm and Rosita Jurgeleit for their patience and help under all bureaucratic circumstances.

It is a great pleasure to thank my friends Cara-Isabel "Isi" Engler, Christina "Tinti" Huber, Georgios "Jorgo" Papanikolau, Anne Sassmann, Christine Schaab, Alexander "Heinzi" Schmidt, Stefan Sojer and many others for their faith, support and the wonderful time I had with them during the years.

Very special thanks go to the honorable members of the Cd19F Franz Fisch, Hubert Krenner, Uli Grasemann and Harald Wenninger. Bobok!

Mein grösster Dank gilt meiner Familie, im Besonderen meiner Mutter und meinem Bruder für die viele Geduld, die große Unterstützung und das beständige Vertrauen, ohne die diese Arbeit nicht möglich gewesen wären.